



STRATAL ARCHITECTURE, LITHOFACIES, ENVIRONMENTAL SETTING, DEPOSITIONAL PROCESSES, AND ASSOCIATED GEOLOGICAL CHARACTERISTICS OF THE UPPER CRETACEOUS AUSTIN CHALK IN LOUISIANA

Robert G. Loucks¹, Christopher K. Zahm¹, Toti E. Larson¹,
Laura C. Zahm², and Peng Zeng¹

¹*Bureau of Economic Geology, University of Texas at Austin,
Box X, University Station, Austin, Texas 78713–8924, U.S.A.*

²*No affiliation, U.S.A.*

ABSTRACT

The Austin Chalk in Louisiana is an active petroleum exploration and production trend. For this siliciclastic-rich chalk to be exploited efficiently, knowledge of the stratal architecture, lithofacies and their distribution, environmental setting, depositional processes, and associated geological characteristics is required. Integration of wireline-log and core data is an excellent method for characterizing this fractured, low-porosity-matrix reservoir system. In the producing trend in Louisiana, the Austin Chalk was deposited in an open-marine, outer shelf setting below storm wave base. Four major lithofacies can be defined that allow analysis of the stratal architecture and stacking patterns within the Austin Chalk. Lithofacies 1 is a highly bioturbated, organic-matter-poor, marly chalk and rarer pure chalk. Lithofacies 2 is a highly bioturbated, organic-matter-poor to -rich, marly chalk to chalky marl. Lithofacies 3 is a slightly burrowed, organic-matter-rich, laminated marly chalk to lesser chalky marl. Lithofacies 4 is an organic-matter-rich, well-laminated marly chalk to chalky marl. Lithofacies 1 was deposited under oxic conditions, lithofacies 2 under oxic to dysoxic conditions, lithofacies 3 under dysoxic to anoxic conditions, and lithofacies 4 under anoxic conditions. Numerous small-scale cycles composed of organic-matter-poor, burrowed units alternating with organic-matter-rich, laminated units are similar to Milankovitch cycles as seen in age-equivalent Niobrara Chalk in the Western Interior Seaway and chalks in the North Sea region in Europe. These cycles are most pronounced in deeper-water, outer-shelf areas away from the regions of uplift. The Austin Chalk pore network is composed of interparticle nanopores between coccolith elements and fewer intraparticle nanopores in clay platelets and inoceramid fragments. Some organic-matter nanopores are within solid bitumen. Organic matter in the chalk is generally type II and III kerogen depending on lithofacies, and some of the chalk has >2 wt% total organic carbon.

INTRODUCTION

The Upper Cretaceous Austin Chalk (Fig. 1) is an oil and gas producing reservoir trend (Fig. 2) and an active exploration target in Louisiana (e. g., Passwaters, 2018; Barnes, 2019; Zborowski, 2019); however, little has been published about the stratal architecture, lithofacies, environmental setting, depositional processes, or associated geological characteristics in the subsurface.

Seven cores from Louisiana (Fig. 3) within the Austin Chalk provide an opportunity for investigation of the subsurface geology and reservoir characteristics of this unit. The Austin Chalk is a siliciclastic-rich limestone to calcareous siliciclastic mudstone that is different from the purer chalks deposited in much of the North Sea region (e.g., Fabricius, 2007) relative to reservoir quality and mechanical properties. This investigation has allowed us the opportunity to study a chalk unit with contrasting lithofacies and mineralogies (i.e., low- to high-siliciclastic content and organic-matter-poor to organic-matter-rich).

The major objective of this investigation is to define some of the geological aspects of the Austin Chalk producing trend in the Louisiana onshore Gulf of Mexico (GOM) area (Figs. 2 and 3). Specific objectives are to (1) define the stratal architecture of the Austin Chalk in the study area, (2) characterize the general litho-

Figure 1. General stratigraphic section of area of investigation. Age plot of Cenomanian–Campanian Supersequence from Phelps et al. (2013). Ages are from Walker et al. (2018).

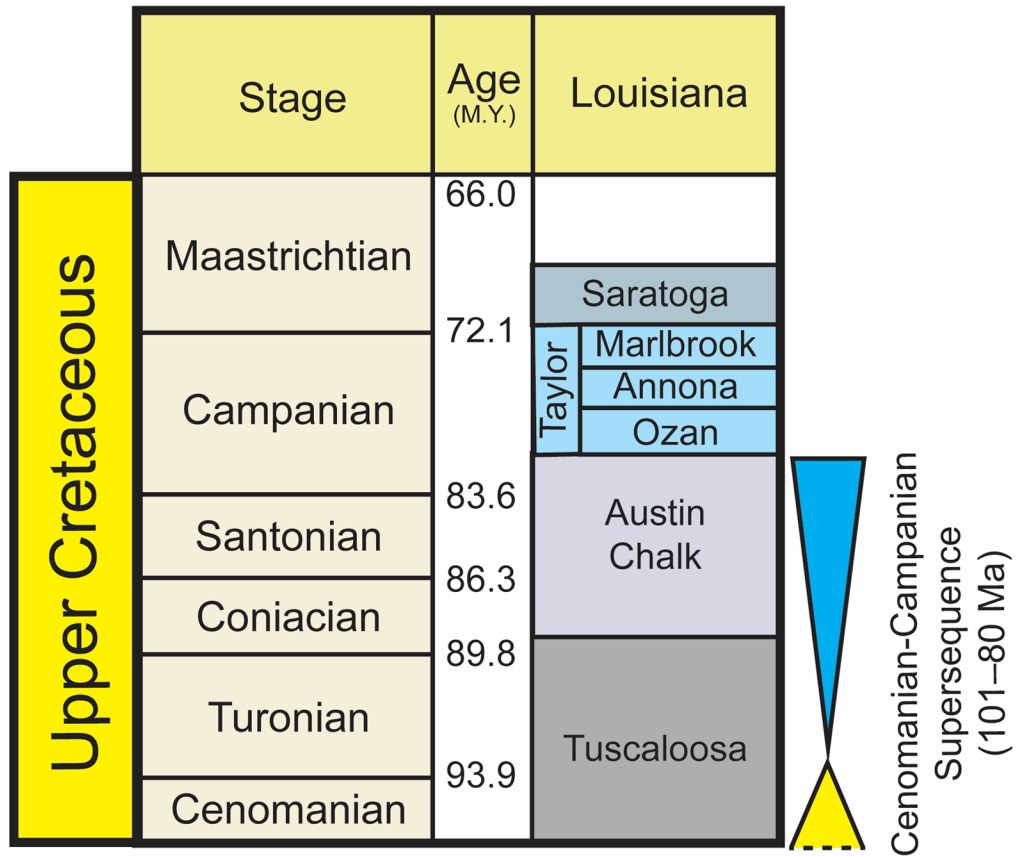
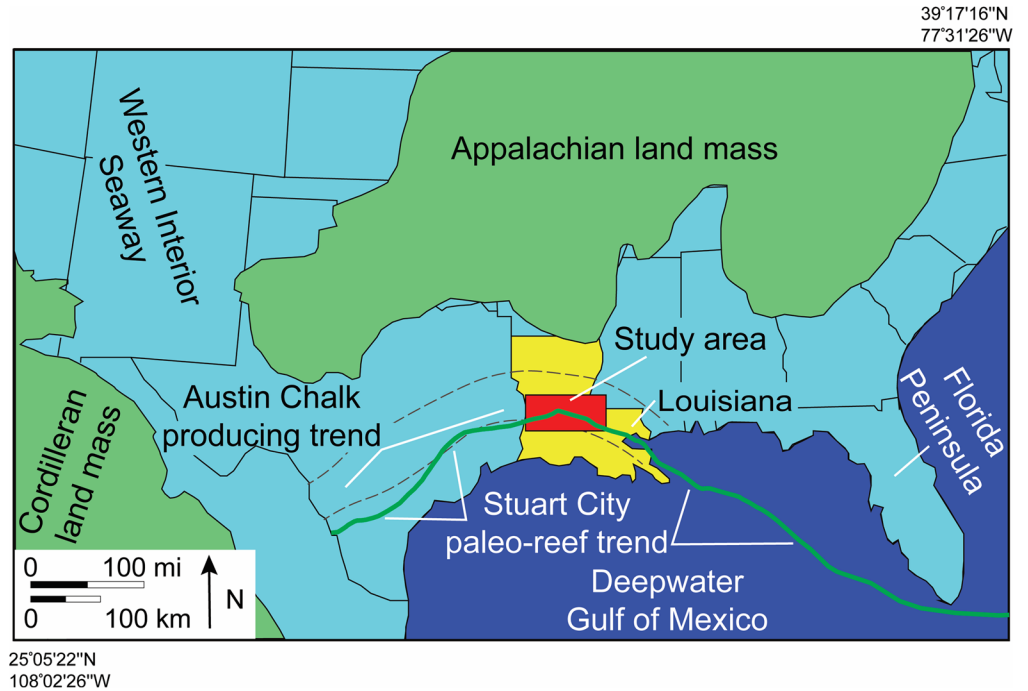


Figure 2. Regional paleogeographic map. Two land masses separated by the Western Interior Seaway were possible sources for terrigenous sediment input into the Austin Chalk. Red rectangle = study area. Dashed lines = Austin Chalk producing trend. Outline of land masses are from Blakey (2011).



facies, (3) provide a review of variable environmental settings and associated schematic depositional models, (4) outline depositional processes, and (5) discuss geological characteristics such as total organic content (TOC), micropetrography (i.e., mineralogy, texture, and fabric at the scale of resolution), pore types, and reservoir quality.

Concepts revealed by this investigation of a siliciclastic-rich chalk will enhance our knowledge of chalk deposition in an area of the subsurface that has had minimal published studies and where several cored sections of the Austin Chalk can be evaluated. Also, information on what controls the wide range in mineralogical composition of this chalk unit can be investigated. This

32°57'21"N
96°01'56"W

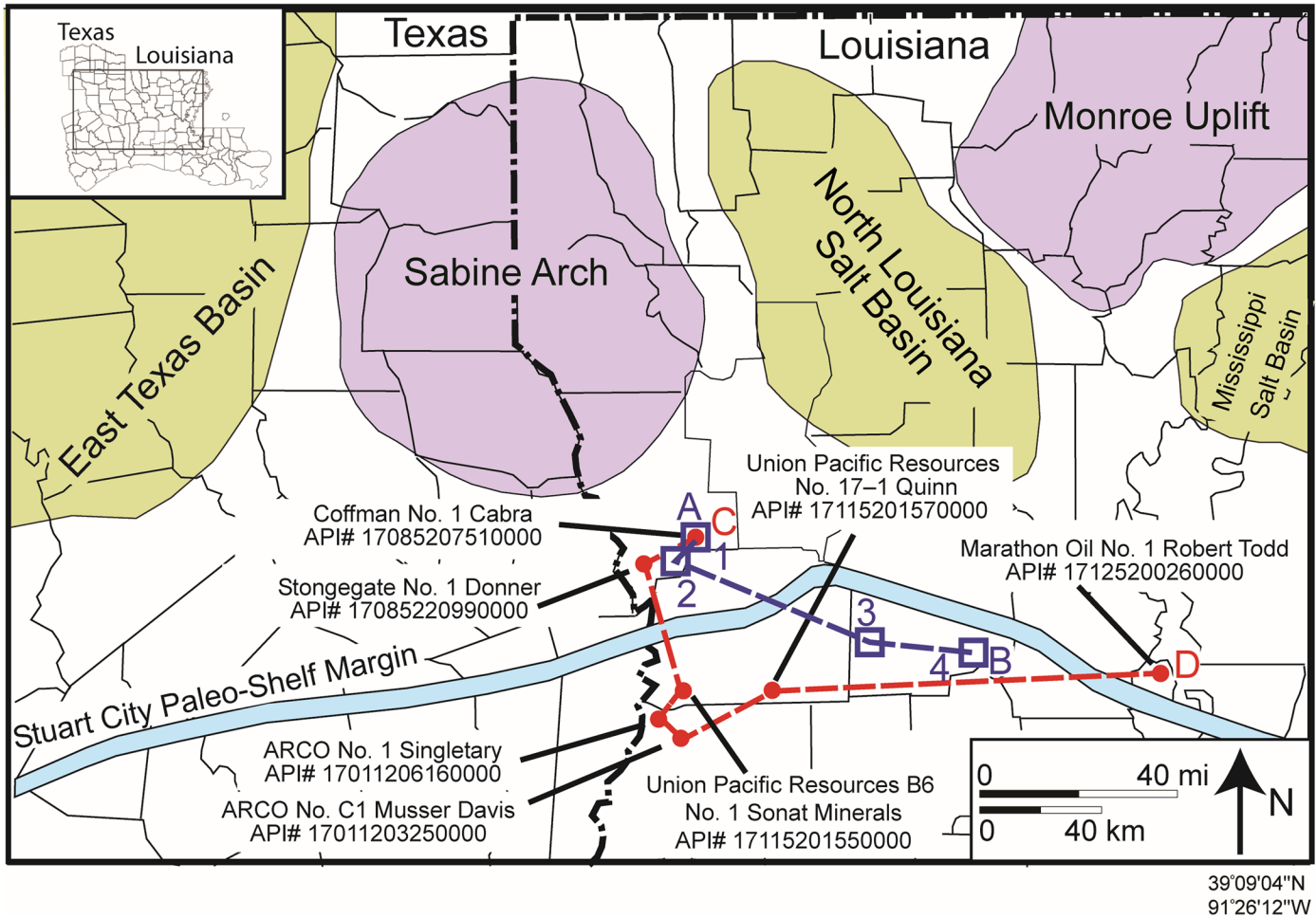


Figure 3. Local paleogeography of area of investigation. Red dots = cores used in study. Blue dashed line = type-wireline cross section A-B (Fig. 7); red dashed line = core cross section C-D (Figure 5). Blue boxes = wells: 1 = Stonegate Production No. 1 Donner, 2 = Texaco No. 1 James Lee, 3 = Chevron No. 1 Burton, and 4 = EOG No. 14-1H Eagle Ranch.

study can thus provide data relative to depositional settings and associated processes of siliciclastic-rich chalks and geological characteristics that are of value in the exploration and exploitation of siliciclastic-rich chalks.

DATA AND METHODS

Rock data for this investigation come from seven cores in Louisiana (Figs. 3 and 4). Wireline logs are available for each cored well, except for the No. 17-1 Quinn core; however, the nearby No. 15 Quinn wireline log can be used to stratigraphically locate the No. 17-1 Quinn core. Relative positions of cores to the top of the Austin Chalk (TAC) are shown in cross-section A-B (Fig. 5). Lengths of core range from 57 ft (17.4 m) to 348 ft (106.1 m), and depths to the tops of cores range from 7000 ft (2133.6 m) to 15,910 ft (4852.1 m) (Fig. 4). Only the No. 1 Robert Todd core recovered a complete Austin Chalk section, with preserved contacts of the Tuscaloosa Shale (below) and the Taylor (above) (Fig. 4). Cores were slabbed so that a flat surface could be viewed and described for texture, fabric, mineralogy, larger biota, and sedimentary features using a binocular microscope. A total of 145 thin sections were analyzed with a petrographic microscope, and thin sections were impregnated with blue epoxy to highlight macropores and blue-fluorescent dye to

highlight nanopores and micropores (using mercury-vapor light).

X-ray diffraction (XRD) analysis was completed on 209 samples by Weatherford Laboratories, which provided weight percentages of major minerals and semiquantitative analysis of clay minerals (Table 1). Mineralogical data were plotted using a chalk classification developed by Loucks et al. (2020b), which emphasizes the apparent mixing trend of carbonate and siliciclastic minerals (Fig. 6). Sample preparation included disaggregating rock chips using a mortar and pestle. A slurry was then prepared and spray-dried onto a mount. Bulk samples were scanned with a Bruker AXS D4 Endeavor X-ray diffractometer using copper K-alpha radiation. Samples were scanned from 5° 2θ to 70° 2θ at a step size of 0.02° per step. Bulk-mineral phases were identified using MDI JADETM 9+ software and the ICDD PDF-4+ 2019 database. For oriented clay-mineral analysis, the >2 micron clay-mineral fraction was dispersed using a Fisher Scientific Ultra Sonifier. The Moore and Reynolds (1997) method was used to identify mixed-layer clay minerals. Kaolinite and chlorite clay-mineral phases were identified by the relative proportions of peaks at 3.59 Å for kaolinite and 3.54 Å for chlorite.

Weatherford Laboratories analyzed 214 samples for total organic carbon (TOC) and pyrolysis parameters (Rock-Eval). Samples were correlated to lithofacies to show the relationship between lithofacies and TOC content.

API# 17085220990000
 Stonegate No. 1 Donner
 Sabine Parish, LA

API#17085207510000
 Coffman Thomas D Inc No. 1 Cabra
 Sabine Parish, LA

API# 17115201550000
 Union Pacific No. 1 Sonat Minerals
 Vernon Parish, LA

API# 17011206160000
 ARCO No. 1 W. W. Singletary
 Beauregard Parish, LA

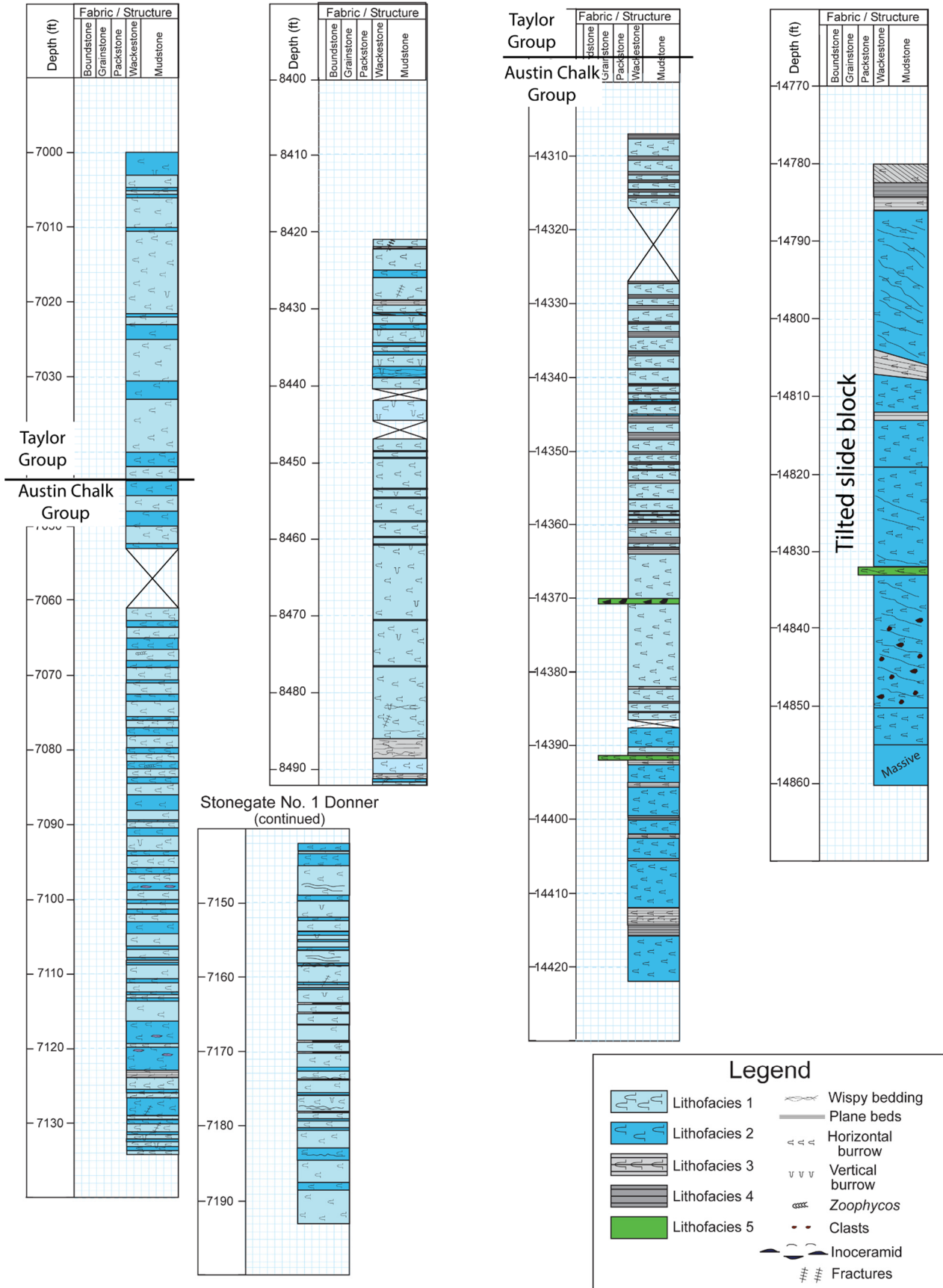


Figure 4. Core descriptions. Continued on **FACING PAGE**.

API# 17115201570000
Union Pacific No. 1-17 Quinn
Vernon Parish, LA

API# 17011203250000
Cortex No. C1 Musser Davis
Beauregard Parish, LA

API# 17125200260000
Marathon No. 1 Robert Todd
West Feliciana Parish, LA

Marathon No. 1 Robert Todd
(continued)

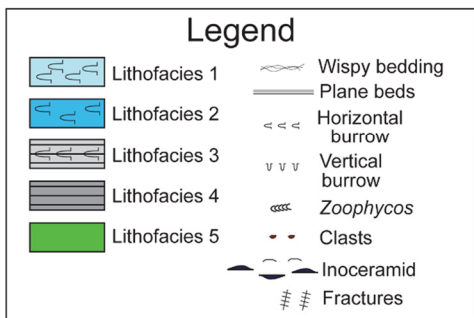
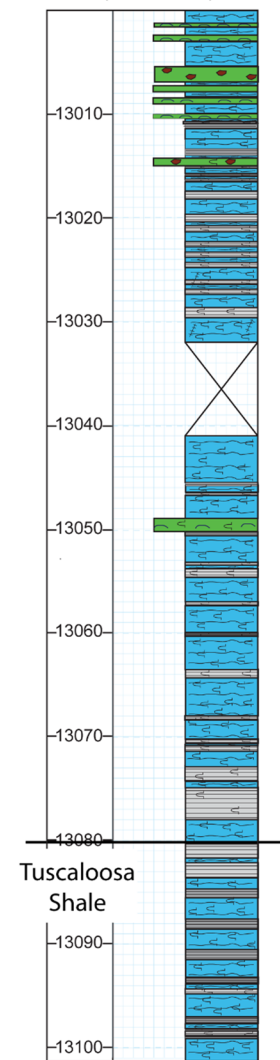
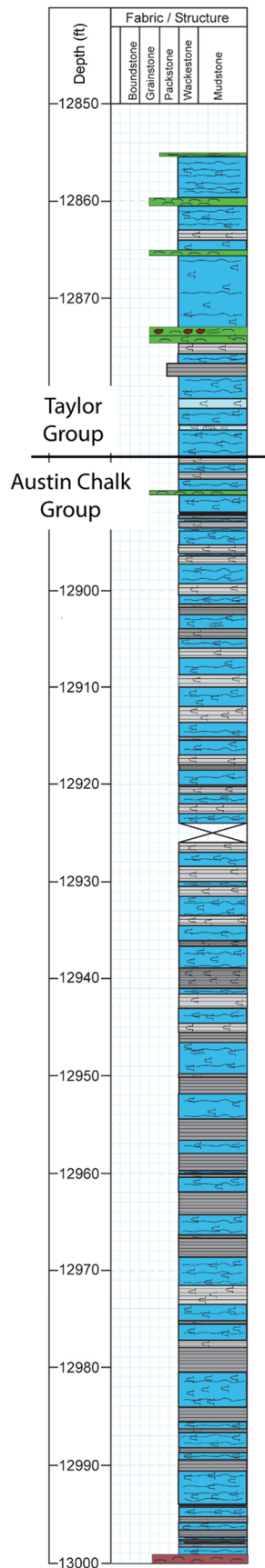
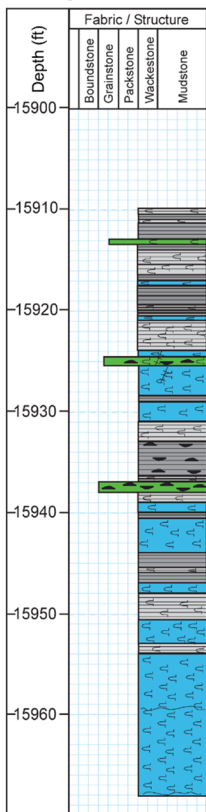
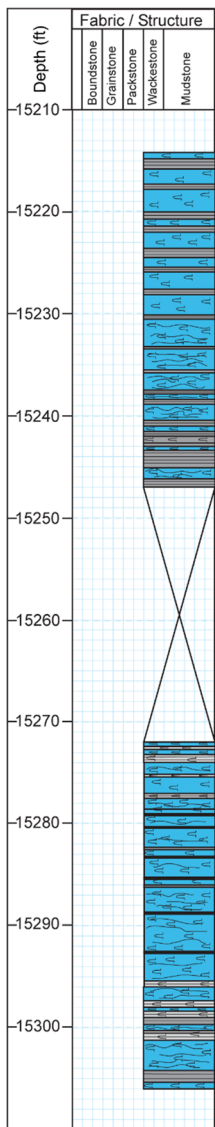


Figure 4, continued. Core descriptions.

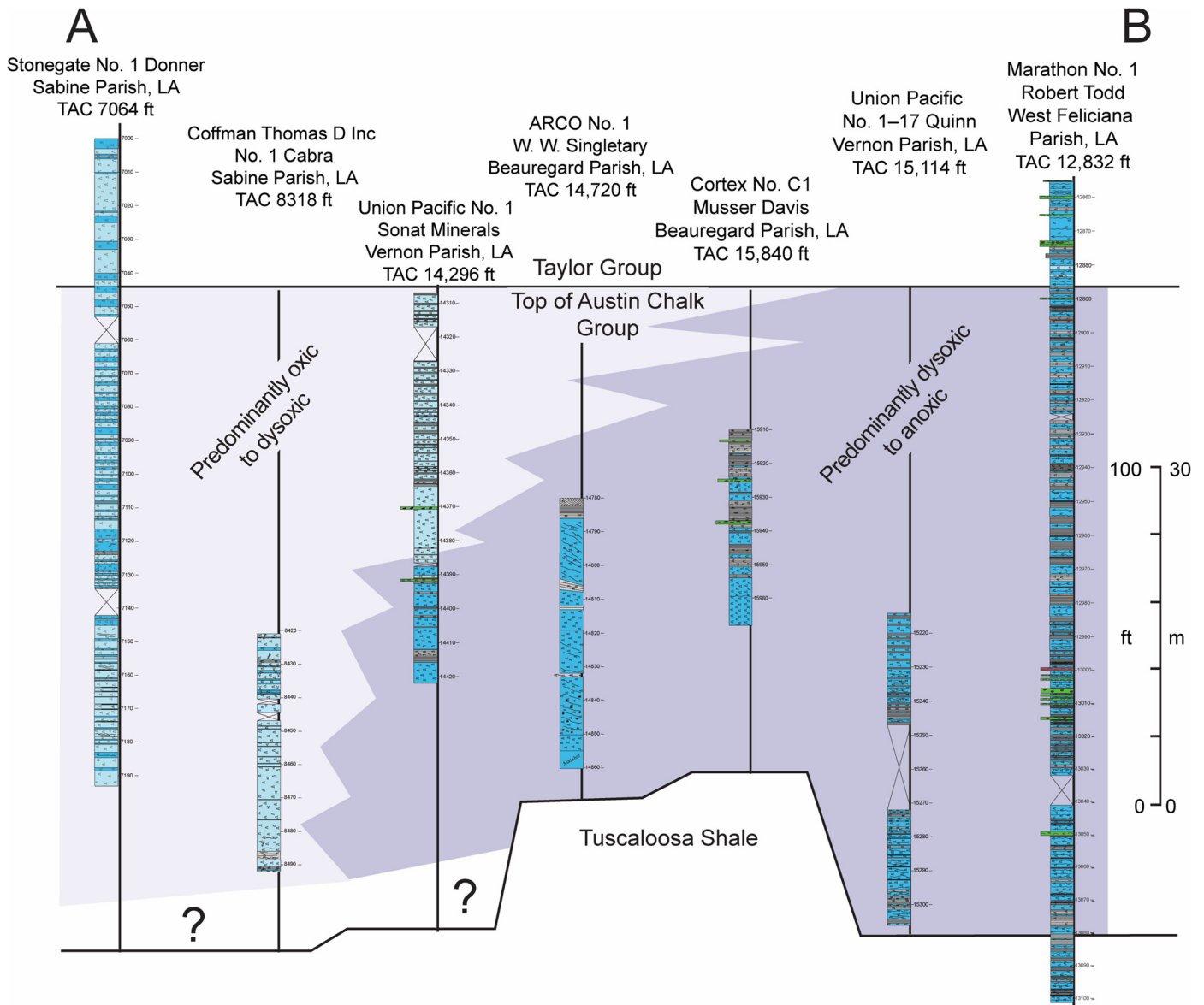


Figure 5. Stratigraphic cross section A–B of cores. Section datumed on top of Austin Chalk Group. See Figure 4 for detailed core descriptions. Note wedge of predominantly dysoxic to anoxic strata in upper Austin Chalk to southwest and east. Location of cross section shown in Figure 3.

Elemental chemical analyses were performed on the No. 1 Robert Todd and No. 17–1 Quinn cores using a hand-held X-ray fluorescence instrument. Elemental concentrations were measured at a 2-in (5-cm) spacing along the core using a Bruker Tracer IV ED–XRF (portable X-ray fluorescence [pXRF]) instrument equipped with an Rh X-ray tube. Excitation voltages of 15 and 40 kV were used for major and trace elements, respectively, with the slabbled core being placed directly onto the nose of the pXRF instrument. Major and trace elements were measured for 60 and 90 s, respectively. X-ray fluorescence measurements were calibrated using methods following Rowe et al. (2012).

One-hundred-thirty core plugs from the No.1 Robert Todd, No. 1 Singletary, and No. 1C Musser Davis cores were analyzed for conventional porosity and permeability. Details relative to the analytical method are unavailable. Also, a total of 47 samples from two wells (No. 1 Singletary and No. 1 Cabra) were analyzed for routine Gas Research Institute (GRI) crushed-core po-

rosity analyses by Weatherford Laboratories. Samples were crushed to 0.5 to 0.85 mm diameter and dried to 212°F (100°C) before analysis. Permeability was not measured. Thirteen samples from the No. 1 Cabra well were selected for special porosity and permeability analysis by a relatively new, highly reliable (especially in the nanodarcy range), modified gas-expansion method (MGE) for measuring tight rocks developed by Peng and Loucks (2016) and Peng et al. (2019) During analysis, helium gas in a pressure tank is introduced to a reference cell. After pressure stabilization, gas is imported into the upper surface of a plug sample installed in a core holder under confining pressure. Helium pressure drops when gas permeates the sample. System volume (i.e., the volume of the reference cell) and dead volumes in both the core holder and tubing are calibrated at different confining pressures, and the averages are used. Permeability can be calculated by the analytical solution of a flow equation from the late-phase pressure data.

Table 1. Table lists the weight percent means of mineral types, separated by lithofacies, in the Austin Chalk Group from X-ray diffraction analysis.

Lithofacies	Calcite		Dolomite		Quartz		Plagioclase		K-spar	
	Mean	S. D.	Mean	S. D.	Mean	S. D.	Mean	S. D.	Mean	S. D.
All data	76.9	16.7	0.02	0.13	3.7	2.2	1.7	0.9	0.07	0.21
1	86.8	15.9	0	0	2.5	1.1	1.6	1.0	0.01	0.07
2	75.3	17.4	0.03	0.16	4.3	2.7	1.7	0.9	0.07	0.25
3	76.7	11.7	0.03	0.18	3.4	1.2	1.6	0.8	0.02	0.12
4	68.3	16.1	0	0	3.4	1.1	1.8	0.8	0.14	0.27

Lithofacies	Mixed-layer clay		Illite/mica		Chlorite		Kaolinite		Apatite		Pyrite	
	Mean	S. D.	Mean	S. D.	Mean	S. D.	Mean	S. D.	Mean	S. D.	Mean	S. D.
All data	7.4	9.3	1.7	2.4	1.0	1.3	1.6	2.8	0.2	0.8	1.6	1.5
1	2.7	2.2	0.6	0.7	0.6	0.7	0.5	0.6	0.1	0.1	0.5	0.6
2	7.4	9.6	1.6	2.5	1.1	1.6	1.4	2.3	0.2	0.9	1.7	1.5
3	8.7	9.1	2.0	2.4	0.8	0.9	1.7	2.1	0.4	0.7	1.8	1.2
4	13.9	11.1	3.2	2.6	1.2	1.1	3.7	5.4	0.3	0.4	2.6	1.6

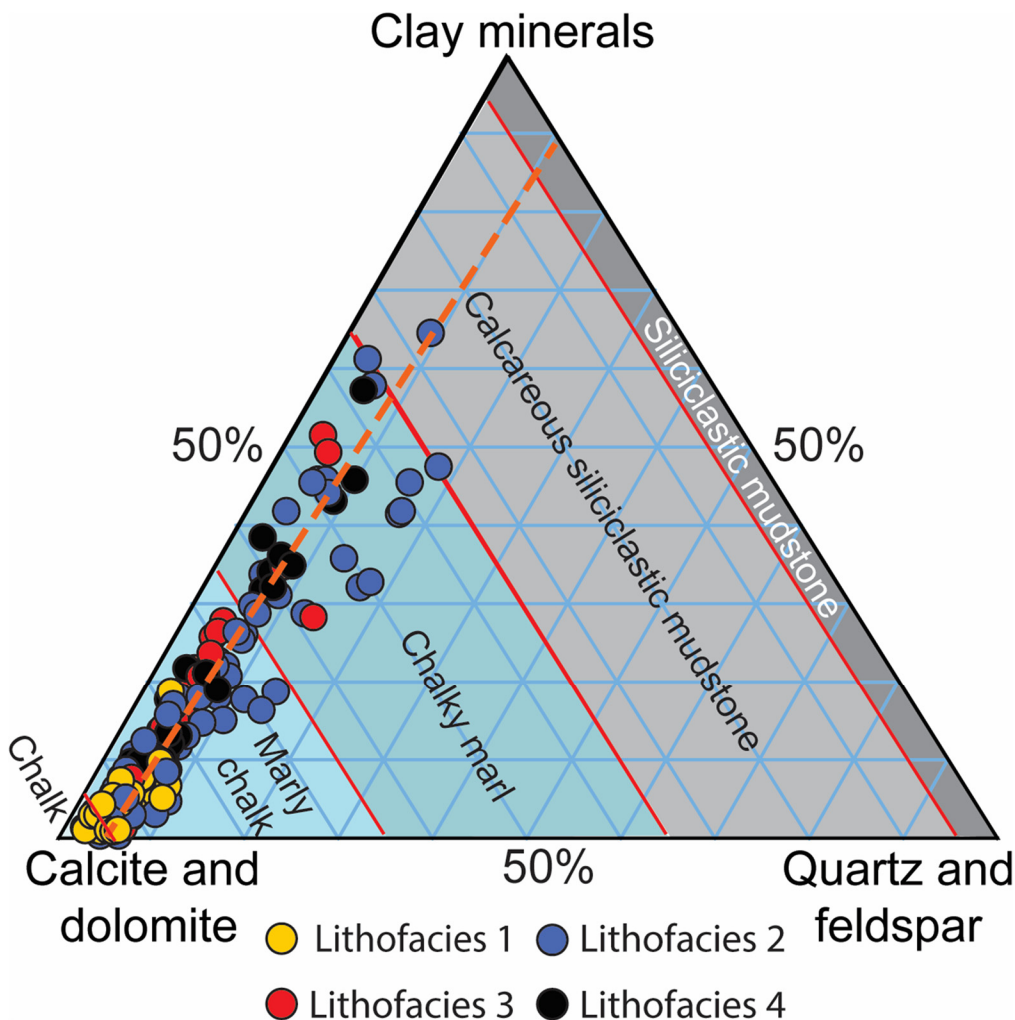


Figure 6. Ternary diagram showing mineralogy based on 209 XRD samples in area of investigation. Samples separated by lithofacies. Red-dashed line indicates mixing trend between carbonate and siliciclastic components. Mineralogy classification scheme for chalks is from Loucks et al. (2000a, 2000b).

AUSTIN CHALK WIRELINE-LOG STRATIGRAPHY

An investigation of subsurface stratigraphy of the Austin Chalk depends on the establishment of acceptable wireline-log correlation markers. The literature reveals no accepted wireline-log stratigraphy or correlation markers for the Louisiana subsurface, although several wireline-log correlation markers have been published (e.g., Anderson, 1979; Goddard, 2001; Louisiana Department of Natural Resources, 2018; Louisiana Geological Survey, 2019), which are inconsistent on a definition of the upper Austin Chalk contact (TAC). Most agree on the base of Austin Chalk contact (BAC); however, Figure 7 shows the variability of wireline-log picks presented for four different proposed Austin Chalk tops as suggested by different studies. This study defines the top of the Austin Chalk (TAC-1) using cores from the No. 1 Donner well in Sabine Parish and the No. 1 Robert Todd well in West Feliciana Parish (Fig. 8). Our study is unique in that the definition of the TAC is core-based; our correlation method for interpreting markers in the Austin Chalk follows.

A regional study by Anderson (1979) constructed a series of cross sections from East Texas into Mississippi, but the emphasis was the northern Louisiana area, not the Austin Chalk producing trend to the south. In one west to east cross section in his Figure 11 that includes Sabine, Vernon, and Rapides Parishes, he correlated a thick Austin Chalk section that ranges from about 600 to 1000 ft (~180 to 300 m). This thickness is much larger than seen in the wells shown in Figure 7. In his cross-section wells, the Austin Chalk section has a lower carbonate-rich interval overlain by a shaley interval. The lower carbonate-rich unit appears to be equivalent to the TAC pick used in this present study.

The BAC correlation pick on wireline logs is straightforward in its definition, showing a strong upward decrease in gamma-ray values from siliciclastic-rich, Tuscaloosa strata below, into lesser siliciclastic-rich Austin Chalk strata above (Fig. 7). Because the TAC is more difficult to define using wireline logs alone, this investigation defines the TAC on the basis of cores from the No. 1 Donner and the No. 1 Robert Todd wells. Cores are interpreted to have recovered the contact between the Austin Chalk below and the Taylor section above (Fig. 8). The Taylor cored section can be identified by a significant increase in siliciclastics relative to the Austin Chalk section in the No. 1 Donner core. The bottom 50 ft (15.2 m) of the Taylor has a siliciclastic mean of 44 wt% according to 9 XRD analyses, whereas the top 50 ft (15.2 m) of the Austin Chalk has a siliciclastic mean of 32 wt% according to 10 XRD analyses. Also, the Taylor section in the No. 1 Donner core is not as cyclically bedded as is the Austin Chalk section. At the correlative No. 1 Donner wireline-log pick in the No. 1 Robert Todd well, the core shows a break from less cyclic strata above in the Taylor, similar to the Donner core, to more cyclic strata below in the Austin Chalk. By comparing cores and wireline logs, we have defined a core-based Austin Chalk upper contact (Fig. 8) that correlates relatively well within the area of investigation (~100 mi [~161 km]). Although this TAC contact is lower in the section than other Austin Chalk picks (Fig. 7), this TAC-1 pick is the only one based on lithologic changes in cores. We consider our correlation pick for TAC to be a “working” TAC pick. The pick represents a change in lithofacies character, and it emphasizes the carbonate-rich Austin Chalk section.

REGIONAL GEOLOGICAL SETTING

The Austin Chalk (group status in the Austin and Dallas areas, formation level elsewhere) is one of several chalks deposited on the deeper water northern Gulf of Mexico platform during the Late Cretaceous. These chalks include the Buda Formation and Eagle Ford/Tuscaloosa Group below and the Ozan, Annona, Marlbrook, and Saratoga formations above (Fig. 1). Phelps et al. (2013) documented that the Austin Chalk is Coniacian to lower

Campanian in age, spanning an ~9 m.y. time period of from 89 to 80 Ma (Fig. 1), and that the Upper Cretaceous platform displayed widespread flooding of the shelf during this period (Fig. 1). Loucks et al. (2020b) estimated that water depth along the area of the Austin Chalk producing trend was >300 ft (>90 m) (outer drowned shelf) on the basis of the sedimentary characteristics of the chalk. According to Blakey's (2011) paleogeographic map of the Upper Cretaceous Gulf of Mexico (Fig. 2), the Florida and Yucatan peninsulas were drowned, and the ancient Gulf of Mexico was essentially an open-oceanic setting. In such a setting, the depth to storm wave base may have been similar to storm wave base (~300 ft [~91 m]) on the east side (i.e., open ocean) of the present-day Florida Peninsula (Reading and Collinson, 1996). As discussed in a later section, sedimentary features and biotas support an open-marine, deeper-water setting, with no effects produced by storm-generated surface waves.

Two major land masses separated by the Western Interior Seaway were possible sources of siliciclastic sediments onto the Austin Chalk drowned shelf—the Appalachian land mass to the north and the Cordilleran land mass to the west (Fig. 2). The Appalachian land mass was the closest to the study area, lying ~60 mi (~100 km) to the north of the area of investigation. Several possible sources of volcanic ash were the western Cordilleran area to the west, the Uvalde Volcanic Field and Travis Volcanic Field in south and central Texas (Baker and Young, 1979; Ewing and Caran, 1982; Dennen and Hackley, 2012), and areas in northern Arkansas (Clark, 1995).

Biotas of predominately coccolithophores, planktic foraminifers, and calcispheres support a deeper-water, outer-shelf, open-marine setting for the Austin Chalk in the study area. Also, bottom-setting conditions varied between oxic and anoxic, as indicated by interbedded burrowed and laminated (i.e., unburrowed) strata.

AUSTIN CHALK GENERAL LITHOFACIES TYPES

Loucks et al. (2020a, 2020b) defined five general lithofacies within the Austin Chalk (Fig. 9). They noted that these lithofacies are present from the Texas–Mexico border to Louisiana. Overall, the unit generally consists of marly chalk to chalky marl, with few pure chalks (Fig. 6). Each lithofacies has a matrix of peloidal coccolith-element hash and clay minerals (Figs. 9A, 9B, and 10). The larger biotas are planktic and lesser benthic foraminifers, calcispheres, inoceramid and oyster fragments, and echinoderm plates.

Lithofacies are defined or characterized by several parameters: (1) depositional features, (2) biotas, (3) mineralogy, and (4) organic matter. Overlap in characteristics is abundant; however, some dominant characteristics prevail that define each lithofacies. Before the five lithofacies are described, some of their parameters are introduced and reviewed.

Depositional Features

Depositional features noted in the Austin Chalk are reviewed in this section, and the integration and significance of these features are presented in the discussion section. Three major classes of depositional features are recognized: (1) burrows, (2) laminations, and (3) gravity flow deposits.

Burrows

Although several studies address bioturbation in the Austin Chalk Group (e.g., Dawson and Reaser, 1990; Loucks et al., 2020b), most studies are from updip outcrops in Texas where the Austin Chalk depositional setting was more oxygenated (e.g., Dravis, 1979) and trace-fossil assemblages are relatively simple, consisting of *Planolites*, *Teichichnus*, *Thalassinoides*, and *Chon-*

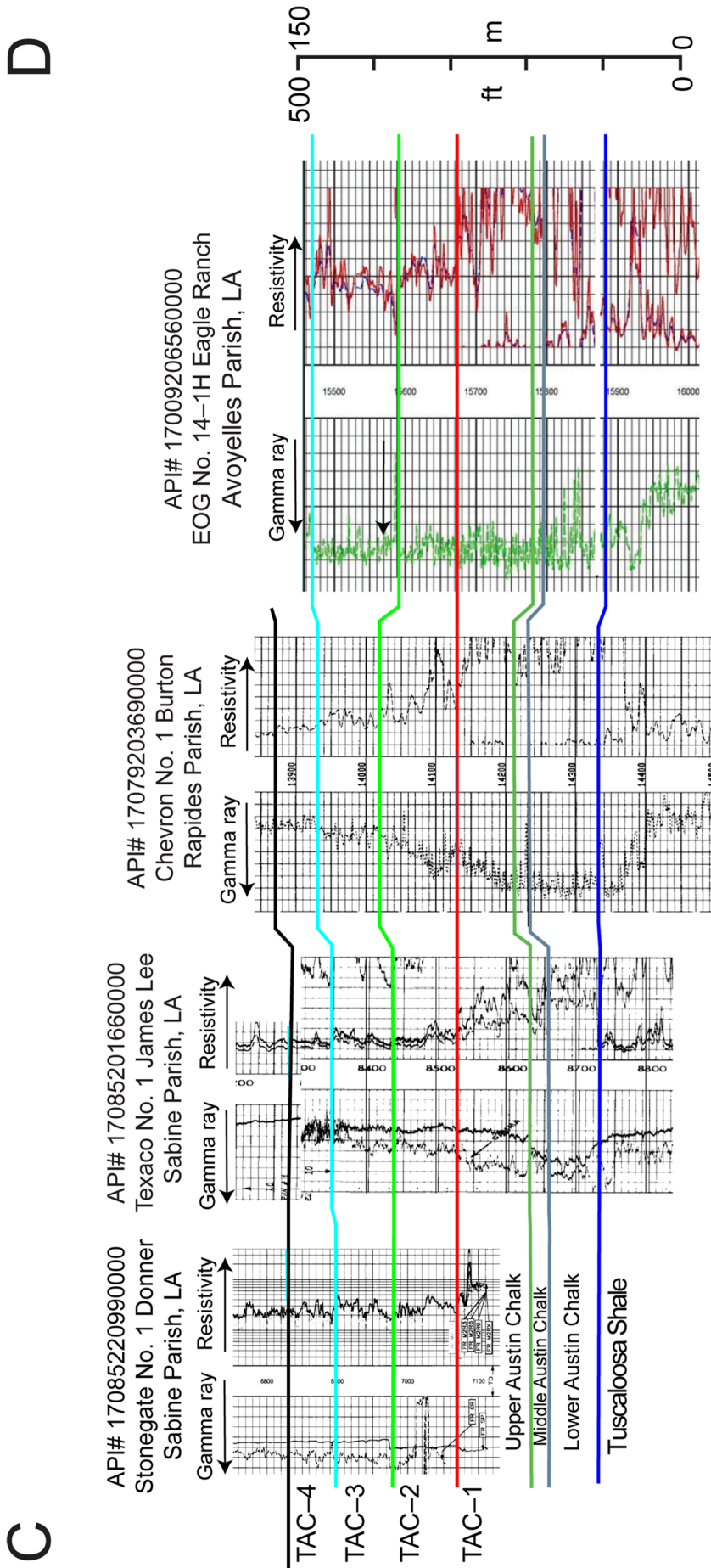


Figure 7. Cross section C–D showing type-wireline logs and associated wireline-log picks. Four wireline logs in the cross section present correlation picks for Louisiana Austin Chalk stratigraphy. Base of Austin Chalk Group pick occurs at sharp upward change from high gamma ray and resistivity to much lower gamma ray and resistivity. Four suggested tops for the Austin Chalk (TAC) are presented. TAC–1 (this investigation) is based on cores in No. 1 Donner and No. 1 Robert Todd wells. This is the only core-based TAC defined, which is used as the working TAC in present investigation. TAC–2 from State of Louisiana Department of Natural Resources (2018) article; Eagle Ranch wireline log from this article. TAC–3 based on correlations from symposium conducted by Louisiana Geological Survey (2019). TAC–4 based on correlations from Goddard (2001). No. 1 Donner well had problems logging at bottom of hole, and no wireline log exists in lowest interval of this well; therefore, the TAC in the Donner well was correlated to nearby No. 1 James Lee well to display the complete section of Austin Chalk Group in that area. Location of the four wireline logs is shown in Figure 3.

C

D

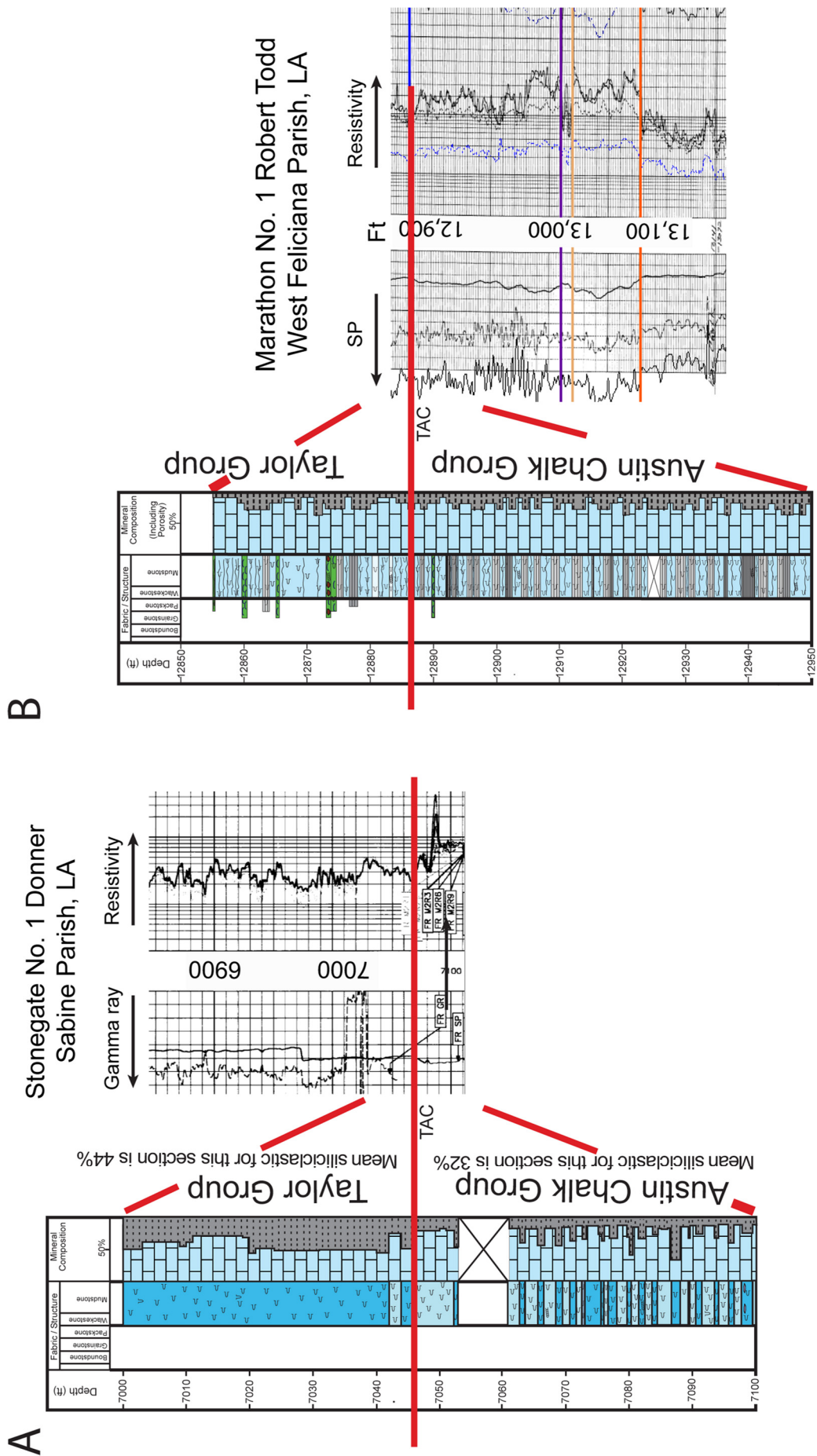


Figure 8. Data supporting core-based top for Austin Chalk Group in Louisiana. (A) Correlation of No. 1 Donner core and wireline log. Core description adjusted slightly to match wireline log (note core depth + 21 ft [6.4 m] = wireline-log depth; measured offset between core and wireline log most likely related to difficulties Stonegate Production encountered in logging bottom of well). Lower half of core description not presented. (B) Correlation of No. 1 Robert Todd core and wireline log. Lower half of core description not presented. See Figure 4A for core symbols. TAC wireline-log pick is correlative in entire area of investigation in Louisiana.

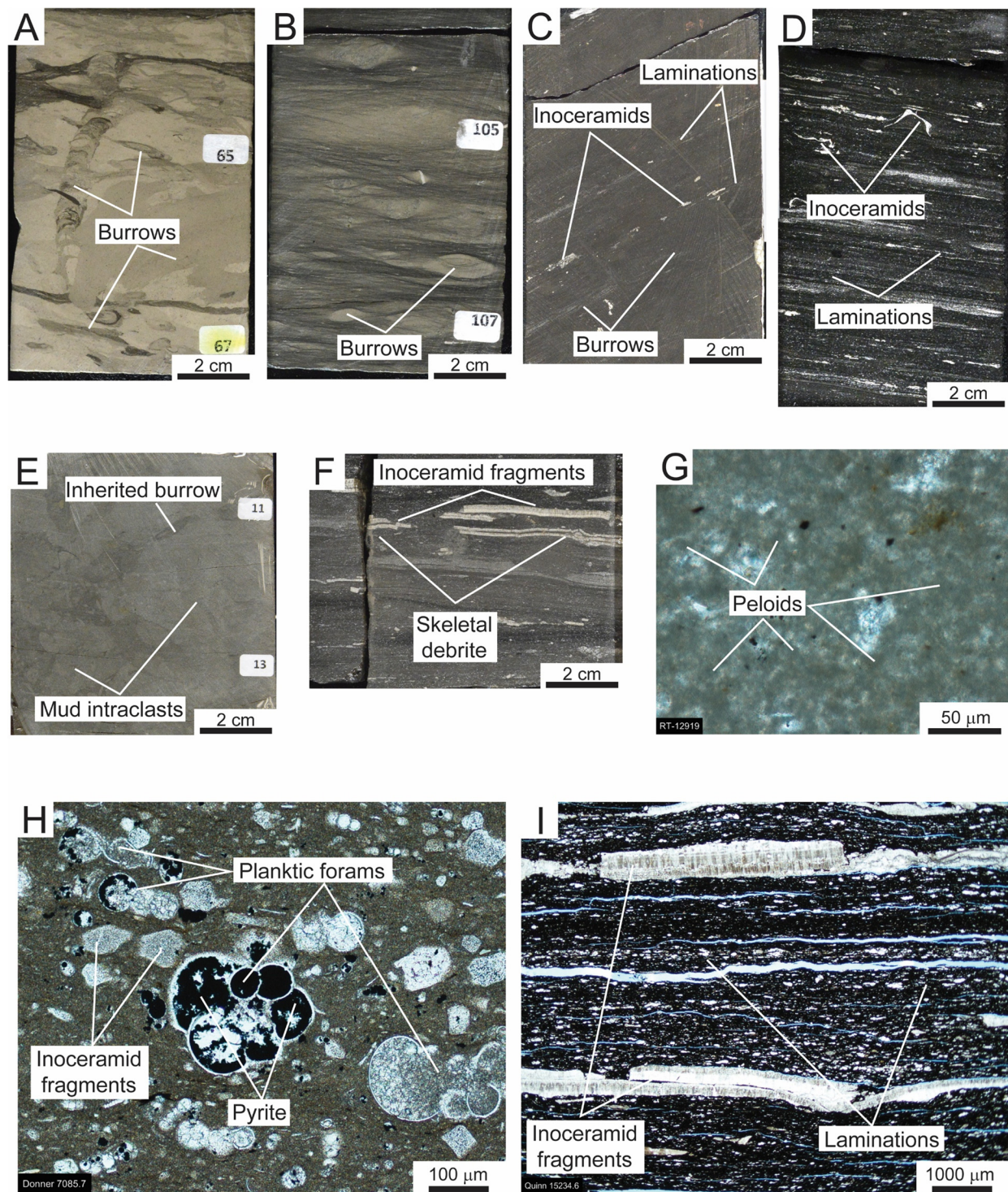


Figure 9. Core slab and thin-section examples of general lithofacies types. (A) Core slab of lithofacies 1: highly bioturbated, organic-matter-poor marly chalk. Note vertical burrow cutting earlier burrows. Stonegate Production No. 1 Donner (7031.0 ft [2225.3 m]). (B) Core slab of lithofacies 2: highly bioturbated, organic-matter-poor to -rich, chalky marl. Sample contains abundant horizontal burrows and solution seams. Stonegate Production No. 1 Donner (7150.5 ft [2179.5 m]). (C) Core slab of lithofacies 3: slightly burrowed (horizontal), organic-matter-rich, laminated marly chalk. Core-slab sample from titled slide block. White grains = inoceramid fragments. ARCO No. 1 Singletary (14,780.0 ft [4504.9 m]). (D) Core slab of lithofacies 4: organic-matter-rich, well-laminated marly chalk. Slab displays compacted inoceramid fragments. Union Pacific Resources No. 1 Sonat B6 (14,330.0 ft [4367.7 m]). (E) Core slab of lithofacies 5: Mud-clast-rich debrite with peloidal coccolith matrix. Some mud clasts contain inherited burrows. ARCO No. 1 Singletary (14,789.5 ft [4507.8 m]). (F) Core slab of thin debrite of inoceramid fragments in lithofacies 4. Union Pacific Resources No. 17-1 Quinn (15,244.0 ft [4646.4 m]). (G) Thin-section example of peloidal matrix seen in Austin Chalk samples. Peloids are probably marine snow. Marathon No. 1 Robert Todd (12,919.0 ft [3937.7 m]). (H) Thin-section example of lithofacies 1 showing planktic foraminifers and inoceramid fragments in coccolith-rich matrix. Pyrite fills several intraparticle pores. Stonegate Production No. 1 Donner (7085.7 ft [2159.7 m]). (I) Thin-section example of lithofacies 4 displaying laminae composed of inoceramid fragments and very fine skeletal hash. Union Pacific Resources No. 17-1 Quinn (15,234.6 ft [4647.2 m]).

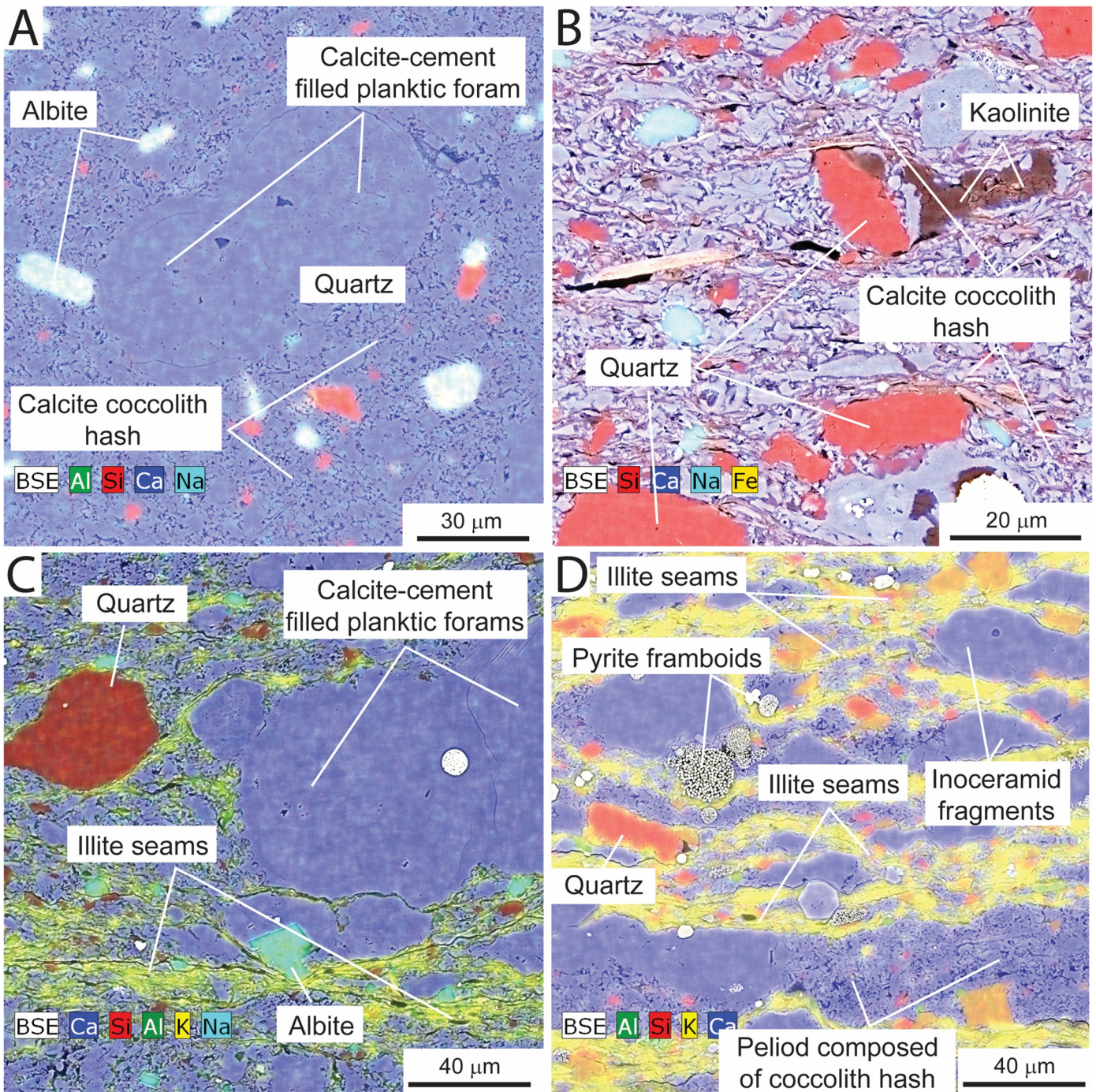


Figure 10. Micropetrography of Austin Chalk samples. All images are from energy-dispersive X-ray spectrometer analyses. (A) Sample is calcite rich, composed mainly of coccolith elements and planktic foraminifers. Planktic foraminifers filled with calcite cement. Some clay- to silt-size quartz and albite present. Union Pacific Resources No. 17-1 Quinn (15,216.4 ft [4637.0 m]). (B) Majority of matrix is calcite coccolith elements. Common quartz silt present; one pore contains authigenic kaolinite. Marathon No. 1 Robert Todd (12,875 ft [3924.3 m]). (C) Sample with clay-mineral-rich (illite) seams showing compaction. Planktic foraminifer and albite and quartz silt grains present. Some calcite matrix coccolith elements. Marathon No. 1 Robert Todd (12,920.0 ft [3938.0 m]). (D) Clay-mineral-rich (illite) sample. Clay forms compacted seams. Larger calcite grains are inoceramid fragments. Pyrite framboids present. Union Pacific Resources No. 17-1 Quinn (15,216.7 ft [4638.1 m]).

drites. Loucks et al. (2020b) studied an outer shelf Austin Chalk core (Getty No. 1 Lloyd Hurt) in South Texas that covered the entire chalk interval and where the bottom waters and sediments ranged from oxic to anoxic. Many trace fossils were identified, and the reader is referred to that study for more detail. The trace

fossils recognized in that investigation were *Chondrites* isp., *Cylindrichnus* isp., *Helicodromites* isp., *Nereites missouriensis*, *Palaeophycus* isp., *Phycosiphon incertum*, *Planolites* isp., *Rhizocorallium* isp., *Schaubcylindrichnus* isp., *Scolica* isp., *Teichichnus* isp., *Thalassinoides* isp., and *Zoophycos* isp. No in-depth

trace-fossil study was undertaken on the Louisiana Austin Chalk cores, but the trace fossils viewed in the Louisiana cores are similar to those noted in the South Texas cores.

Most of the burrows in the Austin Chalk section are horizontal to low angle; however, some vertical burrows in the original oxygenated sediment crosscut other vertical and horizontal burrows, creating tiers (e.g., Fig. 9A). The dominance of horizontal burrows is so intense that in some samples, the rock has a horizontal, pseudo-bedded appearance (e.g., Fig. 9B).

Laminations

A prominent feature in the Austin Chalk is poor- to well-developed laminae (Figs. 9C, 9D, 9F, 9I, 10C, and 10D). These laminae are original depositional features, although partly enhanced by compaction (e.g., become thinner and flatter) of the original mud-rich sediment and are preserved because of the lack of bioturbation. Some laminae are unburrowed (e.g., Fig. 9D), whereas other laminae preserve minor small, horizontal burrows that were not abundant enough to destroy the laminae completely (e.g., Fig. 9C).

The laminae appear to have several origins: (1) suspension-fallout deposits, (2) dilute turbidites, (3) bottom-current deposits, and (4) microbial mats. These features are not always easy to separate according to origin because they can appear similar or can be modified from their original form.

Much of the sedimentation in deeper-water environments is suspension-fallout deposition (e.g., Ewing and Thorndike, 1965). In the Austin Chalk sea, most of the sediment was derived by carbonate biota productivity in the shallower, open-marine water column (few feet/meters to hundreds of feet/meters of water depth, e.g., Hüneke and Henrich, 2011). Also, as discussed later, we suggest that much of the siliciclastic component was delivered by eolian processes as Eldrett et al. (2015) proposed for the Eagle Ford Group, and this siliciclastic eolian sediment would also settle to the sea bottom by suspension-fallout deposition. The actual material that settles from suspension was probably marine-snow aggragates or peloids, as described, for example, by Alldredge and Silver (1988). The matrix in the Austin Chalk commonly appears peloidal (Fig. 9G), the peloids being 10 to 30 microns in diameter and are assumed to be the product of marine snow. Note that the peloids are visible only in thin section, whereas scanning electron microscope (SEM) imaging does not reveal peloids. The ~30-micron thickness of the thin sections allows for observation of thinning of the peloid from its center to its tapering edge.

Another process for sediment transport into the deep-shelf environment is resedimentation of siliciclastic muds or shallower-water chalk sediments. Evidence of resedimented debris-flow deposits, ranging from 1 cm to 1 m in thickness, is evident in the cores. Dilute turbidites, at the millimeter scale as well, also transported these resedimented chalk and siliciclastic materials and contrast with adjacent laminae by grain-size or grain-type differences (e.g., Fig. 9I). Stanley (1993) noted that dilute turbidite laminae are difficult to distinguish from reworked sediment by bottom currents and presented an investigation to separate dilute turbidites from bottom-current deposits. He showed a continuous spectrum from pristine turbidites to fully evolved bottom-current deposits and concluded that bottom currents could effectively rework suspension deposits of marine-snow peloids. The peloids most likely had hydraulic characteristics similar to low-density, silt-size grains.

Another lamina-type is organic-matter layers containing thin, isolated platelets of clay (Fig. 11). These layers are interpreted to be microbial mats similar to those described by Schieber (2007). Comparable microbial mats were described by Loucks et al. (2020b) in a South Texas Austin Chalk core. The mats are microns to tens of microns thick and distorted by compaction. Loucks et al. (2020b, 2021) provided evidence that

these are not compaction-solution seams of organic-matter residue, noting that rip-up clasts of these mats are commonly associated with in-place mats and that rip-up clasts of mats are also present in Louisiana Austin Chalk cores (Fig. 11). The rip-up clasts are evidence that these organic-matter laminae cannot be pressure-solution seams because such seams form during burial. If these organic-matter seams formed during burial, they could not have been exposed at the seafloor to be eroded into clasts. Schieber (2007) provided similar evidence relative to microbial mat rip-up clasts. Also, insoluble residue such as quartz and albite silt, pyrite framboids, etc., were noted in the seams.

Debrites

Besides dilute turbidites, the other type of gravity-flow deposit recognized in the Austin Chalk is thin debrites, which appear as beds formed by mud intraclasts (chalk material) (e.g., Fig. 9E) in a mud matrix (coccolith hash dominated) and has skeletal layers dominated by compacted inoceramid fragments (e.g., Fig. 9F). Fragile inoceramid shells can be transported without fragmenting in debris flows as the supporting mechanism by buoyancy and not turbidity (e.g., Mulder and Alexander, 2001).

Biotas

Biotas are important to an understanding of the depositional setting of the Austin Chalk. Observed biotas comprise predominantly planktic flora and fauna that lived in the offshore, shallower water column in an open-marine setting (Figs. 9, 10, and 12).

Coccolithophores

Coccolithophores, which provide most of the carbonate material that composes the chalk, are marine, unicellular phytoplankton organisms encased in calcite plates or coccoliths (e.g., Guerreiro, 2013), which live in the open-marine shallower-water column, and whose habitat ranges from the surface down to 650 ft (200 m) (Guerreiro, 2013). They prefer still, nutrient-poor water. Individual coccolithophores settle to the bottom of the sea but more commonly settle as agglutinated marine snow and as fecal pellets (Roth, 1994; Steinmetz, 1994; Balch, 2004). Broerse et al. (2000) and Ziveri et al. (2000a, 2000b) showed that coccolithophores begin to break down into coccoliths and coccolith fragments as they descend through the water column.

As seen in SEM images of the Austin Chalk, calcite coccoliths and associated elements compose most of the matrix (Figs. 10A and 10B). Scholle (1977) and Loucks et al. (2020b, 2021) showed that the major diagenetic process that lithifies these Austin Chalk coccolith hashes is calcite overgrowth cementation.

Foraminifera

Planktic foraminifera in the Austin Chalk (Figs. 9H, 12C, 12D, and 12F) in the study area far outnumber benthic foraminifera (Fig. 12F). In fact, planktic foraminifera are present in nearly all samples, whereas most samples have no benthic foraminifera, and only a few samples show a small number of benthic foraminifera. Planktic foraminifera live in a euphotic zone in the marine environment (e.g., Bé, 1960), as they require light for photosynthesis. This limits planktic foraminifera to the upper 650 ft (200 m) of the water column and, generally, to the upper 330 ft (100 m).

On the other hand, benthic foraminifera are bottom dwellers and can live on modern shelves to depths of 1500 ft (500 m) (van der Zwan et al., 1990). The lack of benthic foraminifera in the Austin Chalk is remarkable because, in similar modern platform environments, such as the northern Yucatan Platform near the shelf break at depths of ~405 ft (~150 m), 20 to 60% of the foraminifer population consists of benthic foraminifera (Williams, 1963). Also, benthic foraminifera are common in North Sea

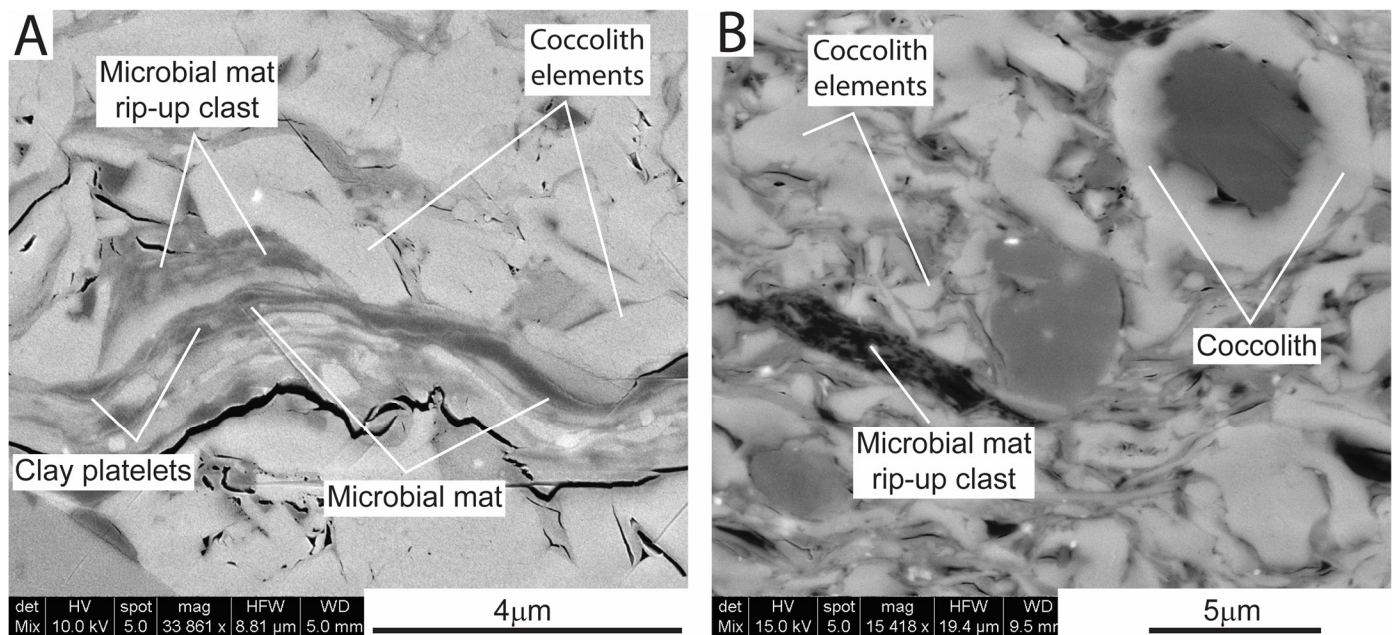


Figure 11. Microbial mats. (A) Compacted organic-matter microbial mat containing clay platelets. Above mat is rip-up clast of microbial mat indicating exposure at sea bottom. Marathon No. 1 Robert Todd (12,290.2 ft [3746.1 m]). (B) Microbial mat rip-up clast with clay platelets in coccolith-element matrix. Marathon No. 1 Robert Todd (12,974.0 ft [3954.5 m]).

chalks (e.g., [Bergen and Sikora, 1999](#)). The low abundance to absence of benthic foraminifers in the Austin Chalk strata suggests very deepwater sedimentation or restricted anoxic bottom waters. Austin Chalk water depths in the area of investigation are thought to be in the range of 300 ft (90 m) to possibly 600 ft (180 m) or more, which is still in the depth range of benthic foraminifers; therefore, the bottom waters must not have been suitable for benthic foraminifers to live.

We do note the occurrence of rare agglutinated foraminifers in beds that contained quartz silt ([Fig. 12I](#)); these foraminifers used this silt to construct their tests ([Fig. 12I](#)). Agglutinated foraminifers can live in deeper-water environments under dysoxic conditions ([Schieber, 2009](#)).

Calcspheres

Calcspheres are calcareous cysts of planktic dinoflagellates, which lived in the shallower part of the water column in the photic zone ([Vink, 2004](#)). [Flügel \(2004\)](#) noted that calcspheres are generally found in deep-shelf to slope sediment and less commonly in inner-shelf sediment. They are common in some Austin Chalk samples ([Fig. 12C](#)).

Inoceramids

Broken fragments and individual elements of inoceramid molluscan bivalves ([Figs. 9D, 9H, 9I, 12D, and 12F](#)) are found scattered throughout the Austin Chalk strata. They are also common in other, deeper-water units of the Upper Cretaceous in Texas, such as the Buda Formation ([Loucks et al., 2019](#)) and the Eagle Ford Group ([Loucks, 2018](#)), although whole specimens are rare. Inoceramids (now extinct) were flat and thin-shelled (with a prismatic-crystal wall structure), which allowed them to live on soft, muddy bottoms without sinking into the mud. They also had large gill areas, which enabled them to survive in oxygen-deficient waters ([Boucot, 1990](#)). The nearly whole to larger shell fragments occur in anoxic, laminated lithofacies, in which the lack of bioturbation precluded the mechanical abrasion of the

shells. In more oxidized lithofacies, burrowers mechanically fragmented the thin, prismatic shells into individual prisms (e.g., [Fig. 12D](#)) or fine fragments composing a few prisms.

Echinoderms

Fragments of both benthic and pelagic echinoderms occur in the Austin Chalk section. The benthic echinoderms are probably echinoids (e.g., [Fig. 12D](#)), and fragments of these organisms are noted in the more oxic strata. The pelagic echinoderms were saccocomids or swimming crinoids (e.g., [Fig. 12E](#)) common in the Late Cretaceous (e.g., [Moore, 1967](#)). They floated in the water column and settled to the bottom after death. Fragments of saccocomids are more common in deeper-water Austin Chalk lithofacies as they favored an open-marine environment

Oysters

Oysters (e.g., [Fig. 12G](#)) occur in the oxygenated Austin Chalk lithofacies, which appear to be sediments deposited in shallower water. Oysters, always found as fragments in the Austin Chalk, can tolerate variations in temperature, salinity, dissolved oxygen, and concentrations of suspended sediments ([South Carolina Oyster Recycling and Enhancement, 2020](#)).

Other Biotas

Rare occurrences of other biotas noted in the Austin Chalk include radiolarians (e.g., [Fig. 12A](#)), ostracods (e.g., [Fig. 12C](#)), and fish detritus (e.g., [Fig. 12H](#)). The radiolarians lived in the outer-shelf, open-marine, shallow-water column, whereas the few ostracods noted were found in strata suggesting shallower-water, oxic deposition. Fish detritus includes scales, bones, and teeth.

Mineralogy Overview

A ternary diagram ([Fig. 6](#)) summarizes XRD mineralogical analyses for the Louisiana Austin Chalk, showing a trend between carbonate (predominately calcite with traces of dolomite)

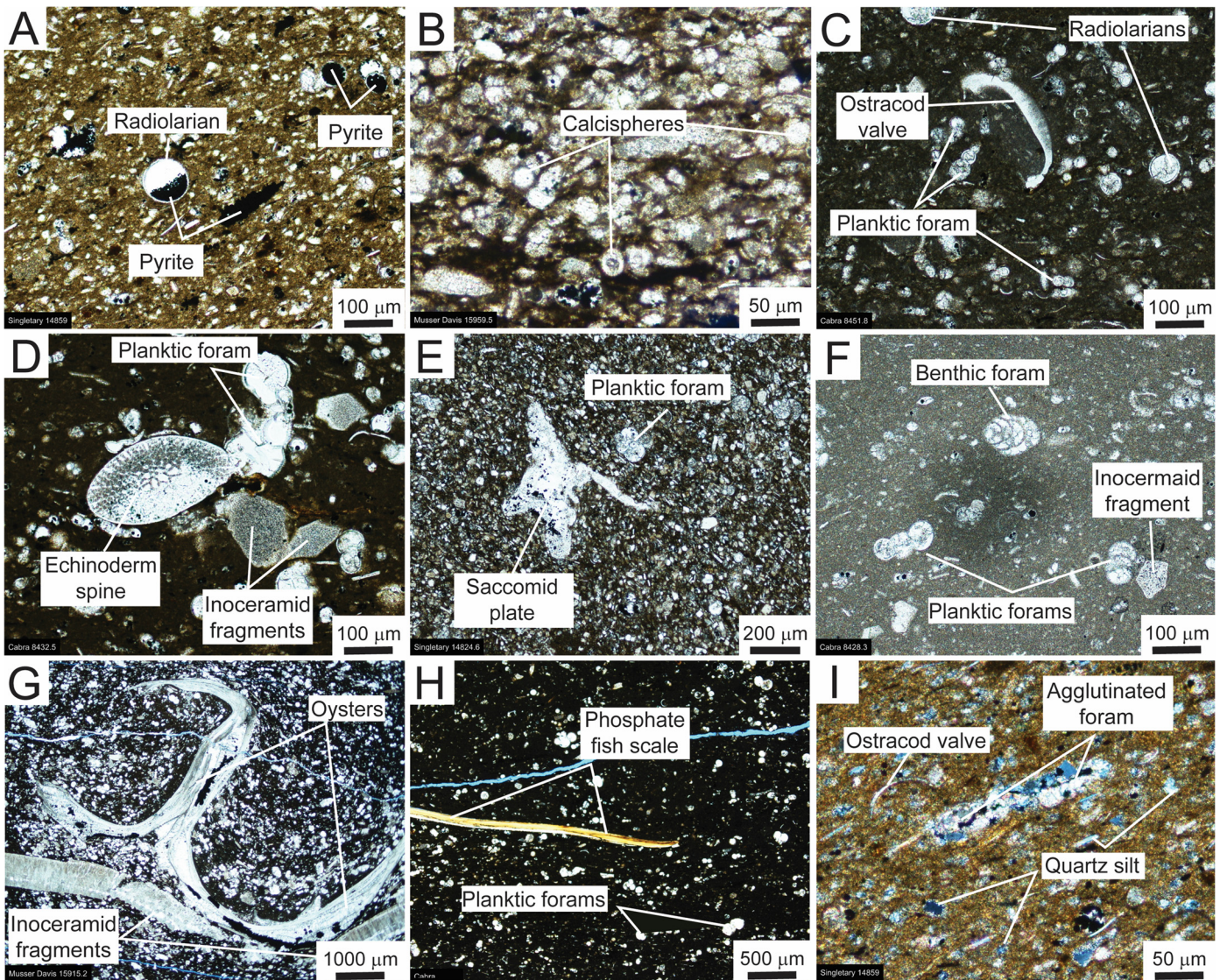


Figure 12. Austin Chalk biotas. (A) Example of radiolarian filled with calcite cement and geopetal pyrite. ARCO No. 1 Singletary (14,859.0 ft [4529.0 m]). (B) Calcispheres filled with calcite cement. ARCO No. C1 Musser Davis (15959.5 ft [4864.5 m]). (C) Planktic foraminifers, ostracod valve fragment, and radiolarians. Coffman No. 1 Cabra (8451.8 ft [2576.1 m]). (D) Larger planktic foraminifer with fragment of echinoderm spine. Individual prisms of disaggregated inoceramids present. Coffman No. 1 Cabra (8432.5 ft [2570.2 m]). (E) Examples of pelagic crinoid (saccoidic) plate. Some small planktic foraminifers present. ARCO No. 1 Singletary (14,824.6 ft [4518.5 m]). (F) Sample contains benthic and planktic foraminifers. Individual inoceramid prism present. Coffman No. 1 Cabra (8428.3 ft [2568.9 m]). (G) Oyster and inoceramid fragments. ARCO No. C1 Musser Davis (15,915.2 ft [4861.6 m]). (H) Example of phosphate fish scale in matrix with abundant small, planktic foraminifers. Coffman No. 1 Cabra (8432.5 ft [2570.2 m]). (I) Agglutinated foraminifer composed of quartz-silt grains. Quartz silt similar to volcanic quartz silt noted in South Texas by Loucks et al. (2020a). Ostracod valve also present. ARCO No. 1 Singletary (14,859.0 ft [4529.0 m]).

and siliciclastic material. A similar trend was noted by Loucks et al. (2020a) for 715 Austin Chalk XRD samples ranging in location from the Texas-Mexico border to Louisiana. Loucks et al. (2020a) postulated that it is a mixing trend and a product of changing ocean chemistry, whereas siliciclastic input remains relatively constant; see that paper for a more in-depth discussion. A preponderance of the Austin Chalk samples in Louisiana is carbonate rich with a majority of samples being more than 50 wt% calcite. Most lithofacies have more than a 5 wt% clay-mineral component, making them impure chalk (pure chalk considered to be <5 wt% siliciclastics). Note that low amounts of clay minerals can affect rock strength. McGinnis et al. (2017) showed that even clay-mineral abundances of 5 wt% can affect rock mechanical properties, and at 10 wt% clay-mineral abun-

dances, the effect on rock mechanical properties is significant. Phosphate minerals in the form of fish-detritus peloids (discussed earlier) and small clasts are also present.

Organic-Matter Overview

Some of the Austin Chalk is rich in organic matter (up to 7 wt% TOC) (Fig. 13). Much of the organic matter is type II kerogen, as shown in a pseudo-van Krevelen plot (Fig. 14). A population of the samples plot in the hydrogen-index (HI) range of the 50 to 150 mg HC/g TOC area (Fig. 14A). These samples are from downdip cores (No. 1 Sonat B6, No. 17-1 Quinn, No. 1 Singletary, and No. C1 Musser Davis), which have higher calculated R_o (i.e., thermal maturity equivalent related to vitrinite re-

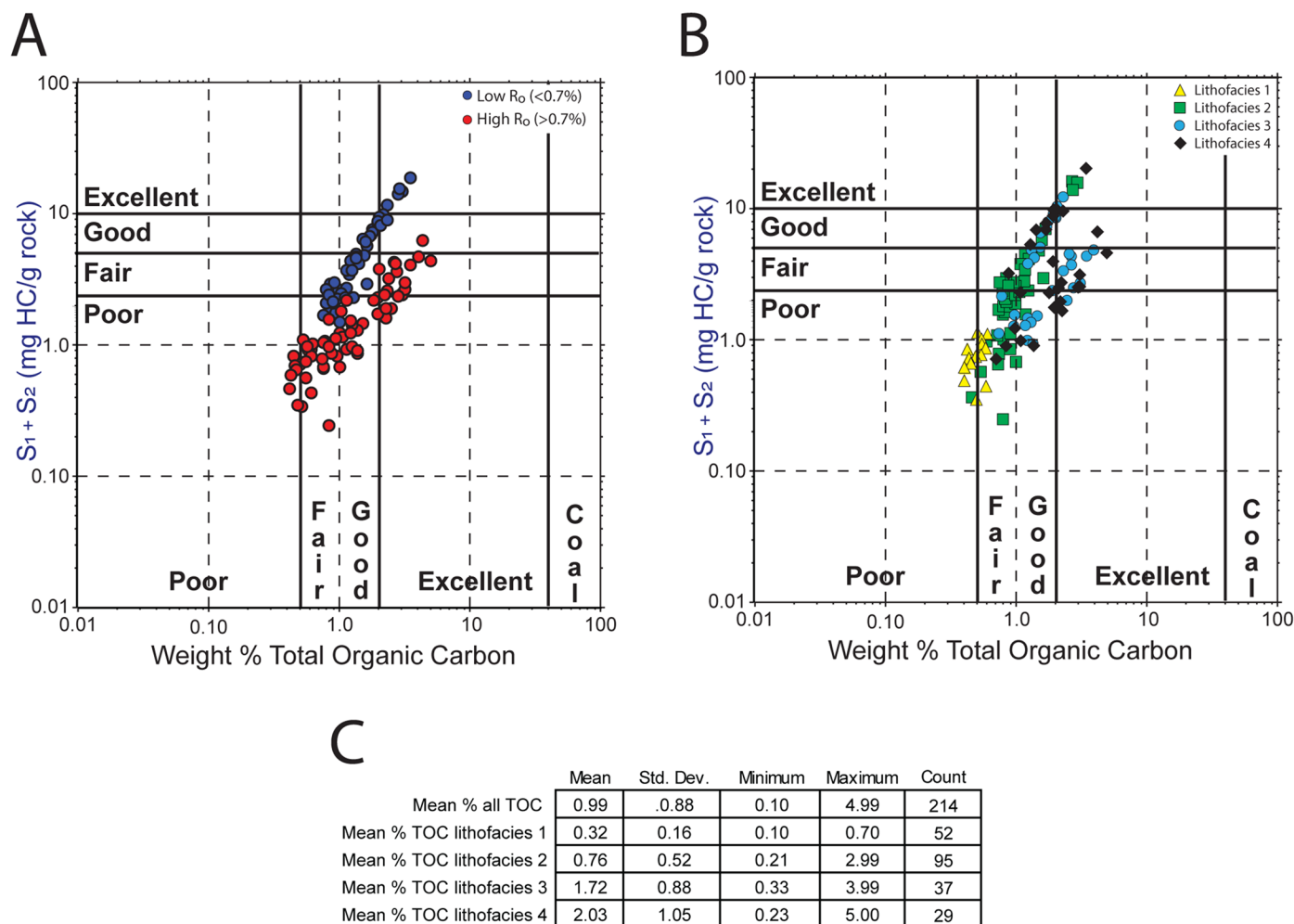


Figure 13. Source rock quality. (A) Plot of $S_1 + S_2$ versus TOC. Data indicate organic matter in many Austin Chalk samples analyzed are fair to excellent source rocks. Two trends noted that are related to thermal maturity. Blue dots are from lower R_o samples and red dots are from higher R_o samples. **(B)** Plot of $S_1 + S_2$ versus TOC where data are separated by lithofacies. **(C)** Percent mean values of total organic carbon (TOC) separated by lithofacies.

flectance) in the range of $>0.7\%$ to 0.9% . These samples probably had kerogen characteristics earlier in their burial history similar to those in core samples from the No. 1 Donner, No. 1 Cabra, and No. 1 Robert Todd wells ($HC/g\ TOC = 150$ to $550\ mg/g$, which have lower thermal maturity ($<0.7\% R_o$). Samples with higher thermal maturity are interpreted to have evolved to the point of expelling much of their hydrocarbon, no longer reflecting original organic-matter composition.

A cross-plot of $S_1 + S_2$ versus TOC (Fig. 13) indicates that many Austin Chalk samples are fair to excellent source rocks, reflecting two trends. Blue dots equal low-maturity (i.e., calculated R_o values $<0.7\%$) samples, and red dots equal high-maturity (i.e., calculated R_o 's $>0.7\%$) samples. Those of lower maturity are just entering the oil window, whereas those of higher maturity are in the early to late oil window. As seen in lower-maturity samples (Fig. 14A), the preponderance of Type II kerogen indicates good-quality algal-based source rock.

General Lithofacies Types

Rock-slab and thin-section examples of all lithofacies are presented in Figure 9. In general, there are no sharp boundaries between the major lithofacies. Lithofacies range from siliciclastic and organic-matter-poor and highly bioturbated to siliciclastic and organic-matter-rich and well laminated. These lithofacies

generally have the same biotic suite, although proportions vary. Along with each lithofacies description, we infer the general depositional environment. In a later section, a more detailed discussion of depositional environments is presented.

Lithofacies 1

Lithofacies 1 is a highly bioturbated marly chalk and lesser pure chalk poor in organic matter (Figs. 6, 9A, 9H, and 13), with fabric ranging from well-defined burrows (Fig. 9A) to totally bioturbated rock, and is generally light-colored. Most burrows are horizontal, whereas deeper-tiered burrows are vertical (Fig. 9A). This lithofacies is the most calcite-rich (Table 1, Fig. 6), and coccolith elements, planktic foraminifer, calcispheres, and inoceramid fragments are common. Some benthic foraminifers, echinoderm plates, oyster fragments, and ostracods are also present.

Mineralogy is dominated by calcite (86.8 wt%), with 4.4 wt% clay minerals, 2.5 wt% quartz, and 1.6 wt% albite (Table 1). Much of the quartz and feldspar are not readily visible in thin sections, but they are observed as micron-sized particles as imaged on the SEM. Pyrite (0.5 wt%) fills foraminifer tests (Fig. 9H) and occurs as micron-sized framboids. This lithofacies contains the lowest amount of TOC, with a mean of 0.32 wt% (Fig. 13C), and the lowest amount of pyrite.

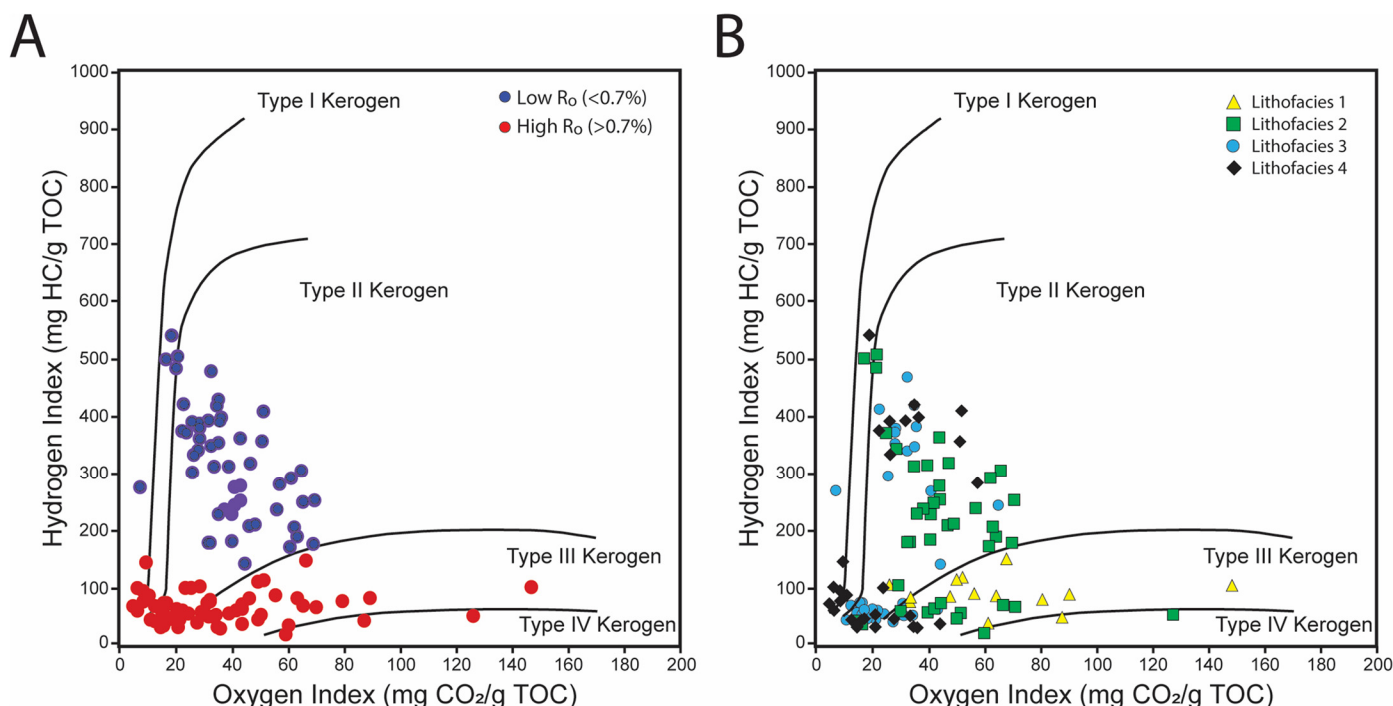


Figure 14. Pseudo-van Krevelen plots of hydrogen index versus oxygen index. (A) Pseudo-van Krevelen plot where data are separated by thermal maturity level. (B) Pseudo-van Krevelen plot where data are separated by lithofacies.

Given the biotas, abundance of burrowing, lack of benthic foraminifers, and relatively low TOC and pyrite content, the depositional environment is postulated to be an oxic, possibly stressed, deeper water setting below storm wave base.

Lithofacies 2

Lithofacies 2 is a highly bioturbated marly chalk to chalky marl with variable amounts of organic matter (Figs. 6, 9B, and 13). A few samples plot as calcareous siliciclastic mudstones. The amount of siliciclastic material varies from ~5 to 75 wt% (Fig. 6), and most burrows are horizontal (Fig. 9B). The intense horizontal burrowing and pressure-solution seams can produce a fabric that appears to be pseudolaminated (Fig. 9B). This lithofacies essentially has the same biota components as lithofacies 1.

Mineralogy is dominated by calcite (75.3 wt%), with 11.5 wt% clay minerals, 4.3 wt% quartz, and 1.6 wt% albite (Table 1). Pyrite (1.7 wt%) fills foraminifer tests and occurs as micron-sized framboids. This lithofacies contains the second-lowest amount of organic matter, with a mean of 0.76 wt% (Fig. 13).

The depositional setting is inferred to be below storm wave base in an oxic to dysoxic setting, given the biotas, abundance of burrowing, moderate TOC, and abundant pyrite.

Lithofacies 3

Lithofacies 3 is a slightly burrowed (horizontal) laminated marly chalk to subordinate chalky marl rich in organic matter (Figs. 6, 9B, and 13). The amount of siliciclastic material is variable, ranging from 5 to 55 wt% (Fig. 6). Most burrows are small, few (millimeters in diameter), and horizontal. This lithofacies has predominately deeper-water, open-marine biotas consisting of coccolith elements, planktic foraminifers, and inoceramid fragments.

Mineralogy is dominated by calcite (76.7 wt%), with 13.2 wt% clay minerals, 3.4 wt% quartz, and 1.6 wt% albite (Table 1). Pyrite (1.8 wt%) occurs as micron-sized framboids that fill foraminifer tests and replaces matrix. Lithofacies 3 contains the second-highest amount of TOC, with a mean of 1.75 wt%.

The depositional environment is inferred to have been deposited in a deeper-water, below storm wave base, dysoxic to anoxic setting, given the laminations, biotas, limited number of horizontal burrows, high TOC, and abundant pyrite.

Lithofacies 4

Lithofacies 4 is well-laminated marly chalk to chalky marl rich in organic matter (Figs. 6, 9B, and 13). The amount of siliciclastic material is variable, ranging from 5 to 63% (Fig. 6). This lithofacies contains predominately deeper-water, open-marine biotas consisting of coccolith elements, planktic foraminifers, and large inoceramid fragments (e.g., Fig. 9D).

Mineralogy is dominated by calcite (68.3 wt%), with ~22.0 wt% clay minerals, 3.4 wt% quartz, and 1.8 wt% albite (Fig. 7). Pyrite (2.6 wt%) fills foraminifer tests and occurs as micron-sized framboids in the matrix. This lithofacies contains the highest amount of organic carbon, with a mean of 2.03 wt% (Fig. 13), as well as the highest amount of pyrite.

The depositional environment is inferred to represent deeper water, below storm wave base, anoxic setting, given the laminations, biotas, lack of burrows, high TOC, and abundant pyrite.

Lithofacies 5

Lithofacies 5 makes up only a minor portion of the Austin Chalk section in the study area (Figs. 4A and 4B). The lithology is variable because the facies is a product of gravity flow processes—mainly debris flows (> 5% clasts) with lesser mud flows (<5% clasts). The depositional fabric is generally described as an intraclast to skeletal floatstone with a peloidal coccolith-rich matrix but ranges from intraclasts in a massive matrix-dominated floatstone (Fig. 9E) to thin layers of skeletal debris (Fig. 9F).

The mineralogy of lithofacies 5 is a function of source material from updip areas. Most fossils are of open-marine biotas, such as planktic foraminifers and coccolith elements. TOC is low (>0.3 wt%) because the unit was sourced from updip oxic areas.

These gravity-flow deposits or debrites are a product of re-sedimentation of updip lithologies into the area of investigation. They are not common and occur randomly throughout the section.

Comparison of Lithofacies 1 through 4

Several trends from lithofacies 1 through 4 can be noted, including an apparent correlation of oxygenation of bottom waters and bottom sediments decreasing from oxic to anoxic. A strong indicator of this trend is the abundance of burrows in lithofacies 1 and 2, small amounts of burrows in lithofacies 3, and no burrows in lithofacies 4. Paralleling this oxic to anoxic trend is a change from no laminae in lithofacies 1 and 2 to moderate- to well-developed laminae in lithofacies 3 and 4. Also paralleling this decrease in oxygenation is an increase in TOC from 0.32 wt% in lithofacies 1 to 2.03 wt% in lithofacies 4.

Mineralogy also displays several trends from lithofacies 1 through 4. Overall carbonate decreases from lithofacies 1 to 4 (Table 1). Clay-mineral content generally increases continuously from lithofacies 1 through 4 (Table 1), from 4.4 wt% in lithofacies 1, 11.5 wt% in lithofacies 2, 13.2 wt% in lithofacies 3, and 22.0 wt% in lithofacies 4. Pyrite, which reflects reducing conditions, also shows an increase in abundance from lithofacies 1 through 4 (0.5 wt%, 1.7 wt%, 1.8 wt%, and 2.6 wt%, respectively).

Trends seen in depositional features, mineralogy, and TOC support the identification of these four lithofacies as the principal building blocks that are significant to understanding stratal and stacking patterns in the Austin Chalk. They allow a consistent lithofacies nomenclature in Louisiana, as well as along the complete Austin Chalk trend. Future studies within the northern Gulf of Mexico Basin may correlate these lithofacies to other properties, such as source-rock richness, mechanical properties, and reservoir quality.

DISCUSSION OF DEPOSITIONAL SETTING AND PROCESSES

Few in-depth studies have been completed on depositional environments and associated depositional processes of the Austin Chalk (e.g., Dravis, 1979; Dawson and Reaser, 1990; Hovorka and Nance, 1994; Dawson et al., 1995; Pearson, 2012; Cooper et al., 2020; Loucks et al., 2020b). The Austin Chalk in the producing trend in Louisiana has generally been regarded as a more or less homogenous section composed of chalk-based rocks with some variation in mineralogy. The present investigation of cores in Louisiana shows that the origin of Austin Chalk lithologies is more complex, although readily understandable when approached from a detailed lithofacies analysis based on rock description and analysis.

Austin Chalk Depositional Setting in Louisiana

Vail et al. (1977) noted that sedimentation of the Austin Chalk occurred during worldwide flooding of Late Cretaceous continental shelves. In the Louisiana area, this flooding produced a series of chalks (Fig. 1) during the Cenomanian–Campanian supersequence (101–80 Ma) defined by Phelps et al. (2013) (Fig. 1); the Austin Chalk is at the upper part of this sequence in the regressive leg. During this time, the area of the Austin Chalk in Louisiana was situated on the drowned outer shelf over 60 mi (100 km) from the nearest landmass (Fig. 2). Clark (1995) documented siliciclastic input (Tokio Sandstone) into southern Arkansas and northernmost Louisiana and interpreted that these lithic-rich sandstones were deposited in deltaic to littoral settings. No sandstone is noted in the Austin Chalk section in the study area, and sand-sized siliciclastic grains are scarce. As discussed earlier, water depths were estimated to be >300 ft (>100 m) and below storm wave base. The shallow part

of the water column was generally open marine and well oxygenated, given the pelagic biotas that lived in this zone. However, as is discussed below, seawater chemistry is inferred to have changed many times during Austin Chalk deposition, given the variations and cyclicity in bottom-sediment types deposited. The Late Cretaceous is characterized by a greenhouse climate where sea-level changes were moderate, generally being less than ~75 ft (~25 m); during the Coniacian, where most cyclic bedding occurs, sea-level fluctuations were generally less than ~35 ft (~12 m) (Ray et al., 2019). These low fluctuations in sea level would most likely not have influenced the deeper water sea-bottom environments in the study area.

Austin Chalk Depositional Models

Loucks et al. (2017, 2019) developed schematic depositional models for the Annona and Buda chalks. The intent of these models was to pictorially present and organize suggested depositional settings and associated depositional processes. In this investigation, these chalk depositional models (Fig. 15) were modified to represent the depositional setting and associated depositional processes for the four main lithofacies, which were defined for the Austin Chalk in the present area. A schematic depositional model for lithofacies 5 is not presented because it is an uncommon, randomly-occurring lithofacies in the Louisiana Austin Chalk, and also because debrite models are well known (e.g., Mulder and Alexander, 2001).

Austin Chalk Lithofacies 1 Depositional Model

A depositional model of lithofacies 1 illustrates a highly bioturbated, organic-matter-poor marly chalk with some pure chalk (Fig. 15A). The general depositional setting was in an open-marine, outer-shelf area far enough seaward to preclude sand-sized siliciclastic sediment. The near-surface, pelagic carbonate factory generated abundant carbonate material that settled by suspension to the deeper seafloor following death. Clay- to silt-sized, siliciclastic sediments are interpreted to have been transported into the outer-shelf area mainly by windblown dust (e.g., continental sediment and volcanic ash), given the fine grain size and lack of any sand-sized siliciclastic sediment. Pelagic carbonate detritus, organic matter, and siliciclastic clay minerals, and fine silt amalgamated into marine-snow peloids, allowing more rapid suspension material. Also, much of the suspended detritus was fed upon by pelagic animals, such as copepods (Hattin, 1975), that digested the coccolithophores and broke them down into coccoliths and coccolith elements, and excreted fecal pellets. These fecal pellets composed of coccoliths are rarely preserved because of bioturbation disaggregating them.

The sea bottom was below storm wave base and unaffected by surface-gravity-wave hydrodynamic processes. Bottom conditions were oxic, but some form of environmental stress must have occurred in the bottom conditions, given the lack of benthic foraminifers and the dominance of horizontal burrows over vertical burrows. Most bottom sediments were composed of pelagic fauna and flora derived from the open-marine, shallow part of the water column. A minor amount of carbonate sediment was contributed by benthic fauna. Some siliciclastic sediment was transported into the area by hemipelagic mud plumes and dilute turbidites, as well as the eolian processes mentioned earlier. Bottom currents and bioturbation reworked much of the sediment. Where the bottom sediment was relatively firm, deeper burrows such as *Thalassinoides* could become established, but in the muddier, less consolidated (i.e., soupier) sediments, horizontal burrows dominated.

Austin Chalk Lithofacies 2 Depositional Model

Figure 15B shows the depositional model for lithofacies 2, defined as a highly bioturbated, marly chalk to chalky marl with

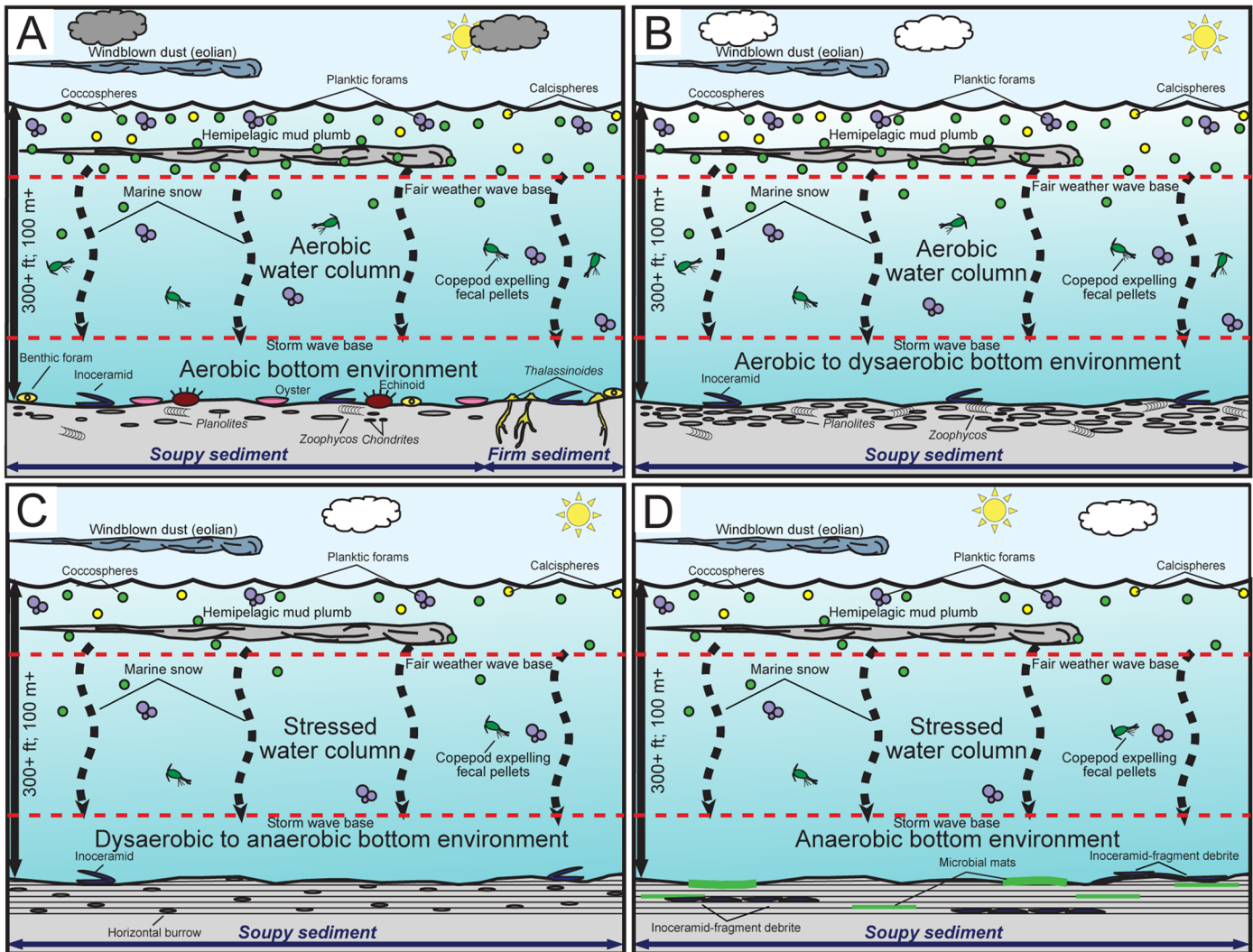


Figure 15. Schematic depositional models for lithofacies 1 through 4. (A) Depositional model for lithofacies 1. (B) Depositional model for lithofacies 2. (C) Depositional model for lithofacies 3. (D) Depositional model for lithofacies 4. See text for discussion of each depositional model.

variable amounts of organic matter. As with lithofacies 1, the general depositional setting was an open-marine, outer-shelf setting below storm wave base. Although the near-surface pelagic carbonate factory was still generating carbonate material, the relative amount of siliciclastic material accumulating appears to have greatly increased (to 65 wt% as compared with only up to 20 wt% for lithofacies 1). The apparent increase in siliciclastic input may be a result of short-term fluctuations in ocean-water chemistry inhibiting high rates of carbonate production. Possibly a decrease in carbonate sediment production allowed for a larger relative percentage of siliciclastic sediment being deposited. When water chemistry promoted high biological productivity, the amount of siliciclastic accumulation was diluted; however, when water chemistry inhibited carbonate production, siliciclastic relative input was enhanced (i.e., not diluted). Evidence shows that ocean-water chemistry ranged from oxic to dysoxic conditions throughout the water column. A plot of pyrite versus siliciclastic content for lithofacies 2 shows a modest positive correlation ($R = 0.63$) (Fig. 16A), and a plot of TOC versus siliciclastic content shows a weak positive correlation ($R = 0.27$) (Fig. 16B). Note that because both pyrite and TOC are commonly correlated with decreasing oxygenation or increasing redox conditions, we can infer that an increase in clay-mineral content may be associated

with a decrease in the quality of ocean-surface water (i.e., lower oxygen levels) and that a decrease (dilution) in clay-mineral content may be associated with an increase in ocean-surface-water quality. In a later section, a suggestion that orbital climatic cycles affected ocean-water chemistry in the Austin Chalk strata will be discussed.

The greater abundance in siliciclastic sediments could also be related to a larger influx of siliciclastic material and not just a lowering of carbonate production. As in lithofacies 1, the siliciclastic component is very fine-grained and probably deposited by eolian transport or hemipelagic processes. Unfortunately, no data about environmental conditions on the Appalachian land mass to the north exist that would suggest a change in the rate of sediment dispersed from this area. Clark (1995) documented that the Tokio Sandstone in northern Louisiana and southern Arkansas had a volcanic source farther to the north, but he did not elaborate on the volcanic source. Ash beds or ash-bed components are scarce in the Louisiana Austin Chalk Group cores; however, if present, the volcanic material is probably extensively altered and difficult to recognize. We may have recognized some volcanic quartz grains in a few samples (Fig. 12I). Also, a lithofacies 2 sample has a kaolinite value of 24 wt% and two lithofacies 4 samples show kaolinite values of 13 and 14 wt%. Further,

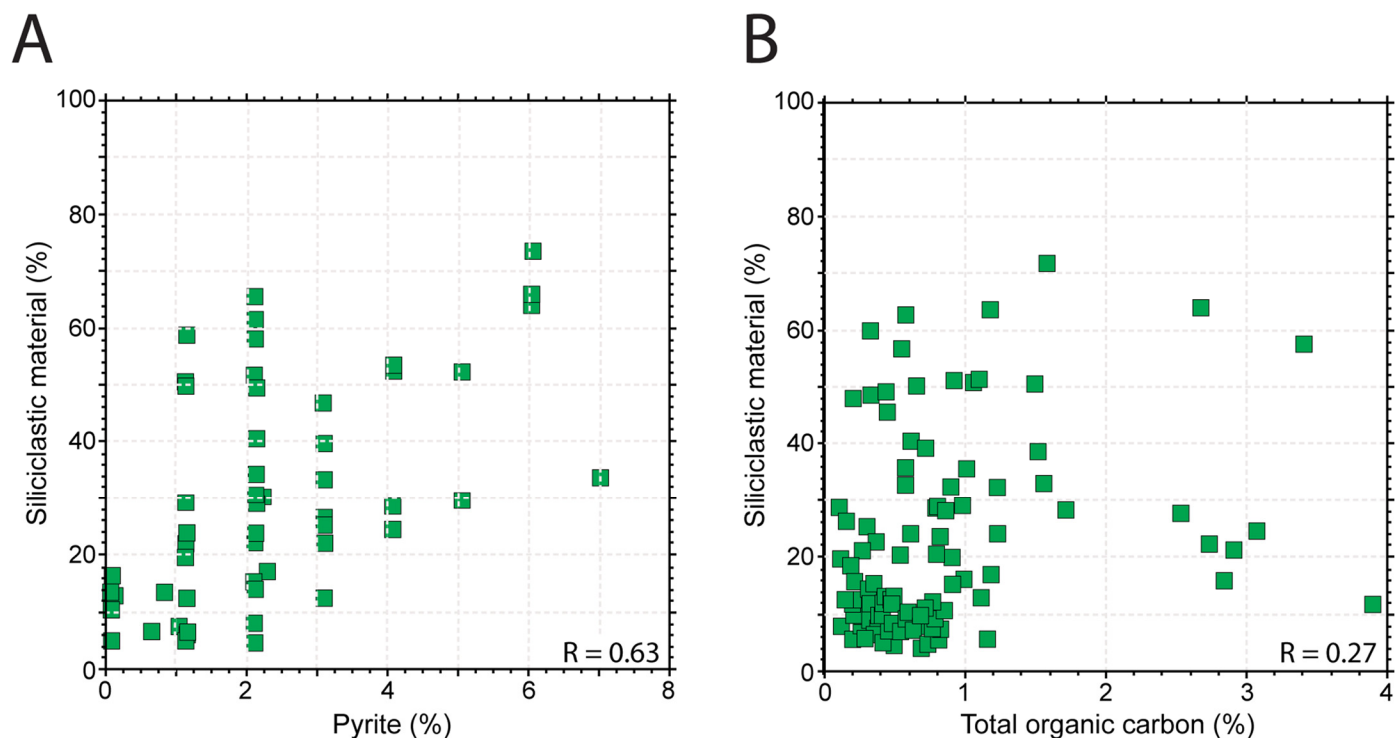


Figure 16. Plots of pyrite and total organic carbon versus siliciclastic material for lithofacies 2. (A) Plot of siliciclastic material versus pyrite. Fair positive correlation between the two parameters. (B) Plot of siliciclastic material minerals versus total organic carbon. Weak positive correlation between the two parameters.

20 samples composed of lithofacies 2 to 4 show elevated kaolinite values of above 5 wt%. The kaolinite could be the alteration product of volcanic ash, as commonly seen in the Eagle Ford Group (e.g., Loucks, 2018).

Depositional processes were generally similar to those in lithofacies 1. Besides the relative increase in siliciclastic abundance, the other difference in lithofacies 2 as compared with lithofacies 1 is the increased amount of TOC and pyrite and the near absence of vertical burrows such as *Thalassinoides*. The abundance of bioturbation in lithofacies 2 suggests oxic bottom water and sediment conditions. Still, the lack of vertical burrows and increased TOC and pyrite suggest increased reducing conditions and some periodic dysoxic conditions.

Austin Chalk Lithofacies 3 Depositional Model

Lithofacies 3 is a slightly burrowed, laminated marly chalk to lesser chalky marl rich in organic matter (Fig. 15C). Lithofacies 3 marks a major change in environmental conditions throughout the water column. Bottom-sediment conditions show a strong change from oxic/dysoxic to dysoxic/anoxic environments, given the preponderance of laminated sediments, high TOC, and abundant pyrite. The general biotas and depositional processes remain similar to those of the previous lithofacies. However, water chemistry appears to have changed to stressed conditions that slowed carbonate production and prohibited extensive bioturbation.

In lithofacies 3, sediment is somewhat to moderately laminated, with some small horizontal burrows. Although the laminated sediment suggests stressed dysoxic to anoxic conditions, the horizontal burrows indicate some oxygenation periods. The bottom environment probably ranged between dysoxic and anoxic. The enhanced redox conditions in lithofacies 3 promoted the preservation of TOC and produced a potentially good source rock.

In this deepwater setting, the upper water column is also thought to have changed in water chemistry, which probably did not continuously favor carbonate production. The lower production rate enhanced the relative amount of siliciclastic sediment abundance (i.e., not diluted) because the siliciclastic volume is assumed to have remained constant (Loucks et al., 2020a, 2020b).

Austin Chalk Lithofacies 4 Depositional Model

The depositional model for lithofacies 4 (Fig. 15D), which is a well-laminated marly chalk to chalky marl and rich in organic matter; is similar to lithofacies 3. Lithofacies 4 appears to have been deposited in a fully anoxic setting. The major differences from lithofacies 3 are the near total absence of burrows and the common appearance of microbial mats, as well as thin, compacted inoceramid debris. The depositional setting for lithofacies 4 was anoxic at depth, in which the only life possible was chemotrophic microbial mats. All the skeletal material noted was deposited from the open-marine, shallower, oxygenated water column or was transported to the area by debris flows. As already mentioned, these debris are characterized by large fragments of inoceramid shells, which were preserved because of the lack of bioturbation that would have fragmented them.

LATERAL ARCHITECTURE AND SMALL-SCALE CYCLES

The Austin Chalk lithofacies defined in this investigation form the basis for describing several spatial and temporal trends in the Austin Chalk across Louisiana. For example, a large-scale regional oxic to anoxic trend is evident from northwest to southwest and east, and vertical, short-term oxic to anoxic trends or cycles can be found in each core. Each of these trends and cycles

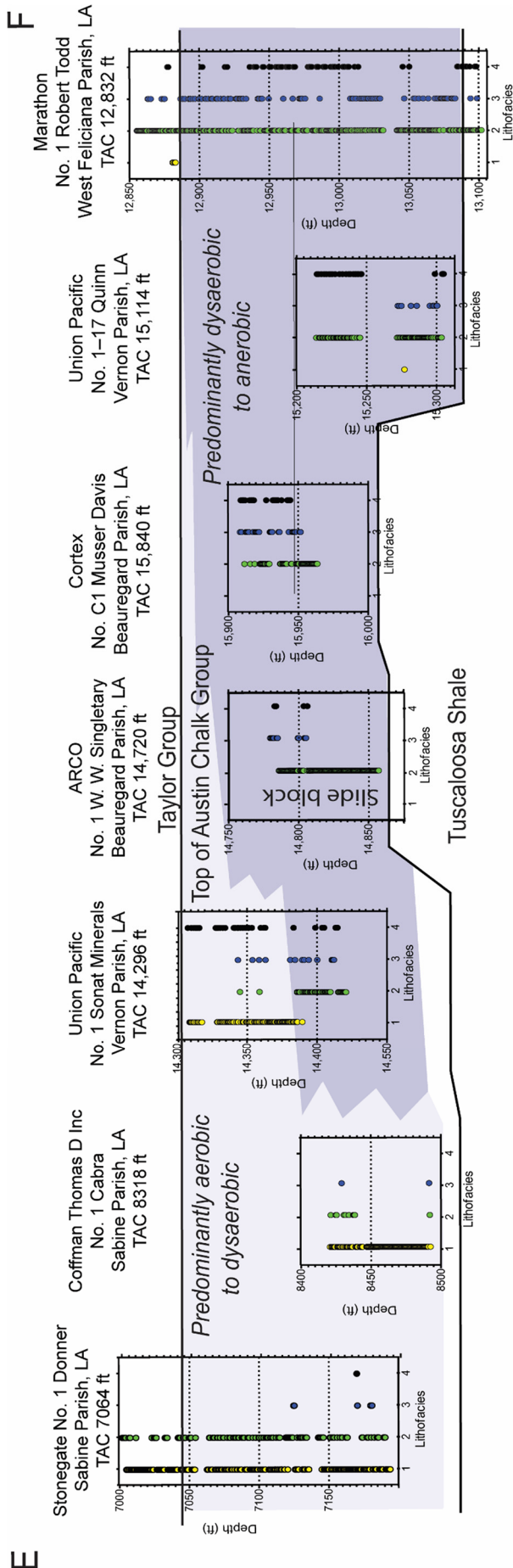


Figure 17. Lithofacies-stacking-pattern stratigraphic cross section. Cross section E-F layout is the same as cross section A-B shown in Figure 5. Lithofacies stacking patterns plotted instead of core descriptions. Each stacking pattern plot shows vertical distribution of lithofacies (see text for details). Notice that lithofacies 1 is more common on the left side of the cross-section and lithofacies 3 and 4 increase to the right along the cross section. Lithofacies stacking pattern plots for the Austin Chalk Group were developed by Loucks et al. (2020).

are defined by variations in lithofacies and major and trace elements.

Lateral Austin Chalk Architecture in Louisiana

Figures 5 and 17 are stratigraphic cross-sections using the same wells, datumed on top of the Austin Chalk. Figure 5, as already noted, shows the relative stratigraphic positions of cores and highlights the dysoxic to anoxic sedimentary wedge in the eastern part of the cross-section. Figure 17 is a similar cross-section, but instead of core descriptions, we used stacking-pattern plots, which are plots of lithofacies versus depth by half-foot picks. This type of stacking lithofacies display was developed by Loucks et al. (2020b). Stacking-pattern plots show the vertical distribution and dominance of each lithofacies through the cored section of the well.

Within the 100 mi long (160 km long) cross-section, note the overall northwest to southwest and east trend, in which lithofacies 1 and 2 are common in the cored sections to the northwest (No. 1 Donner and No. 1 Cabra) and lithofacies 3 and 4 are common in cores to the southwest and east (No. C1 Musser Davis, No. 17-1 Quinn, and No. 1 Robert Todd). In the No. 1 Sonat B6 core, in the southwest, the lower cored section lacks lithofacies 1, and the upper cored section has a mixture of lithofacies 1 and 4. The No. 1 Singletary core, also in the southwest, is a large slide block that is dominated by titled and slightly contorted beds of lithofacies 2. The simplest explanation for this trend is an expected deepening in the water column from the Sabine Uplift area in the northwest to the outer shelf in the southwest and southeast (Fig. 3). However, throughout the area of the cross section, all lithofacies are the result of deeper-water deposition, as noted by the predominance of pelagic biotas, especially the abundance of planktic foraminifers and the coccolith-hash matrix of the chalk. This trend corresponds to the same type of general facies trend described by Dravis (1979) and Cooper et al. (2020) in San Marcos Arch area in Texas.

Small-Scale Cycles in the Austin Chalk Group in Louisiana

Many Austin Chalk cores from the Texas-Mexico border into Louisiana (Loucks et al., 2020b) show small-scale cycles (inches to feet; decimeters to meters) between generally burrowed lithofacies 2 and laminated lithofacies 3 and 4 (Fig. 18). An exception to this cyclicity is seen in the upper half of the No. 1 Sonat B6 core, where lithofacies 1 is interbedded with lithofacies 4 (Fig. 4A). Figure 18C shows a core description of a 50 ft (15.2 m) section from the No. 1 Robert Todd well, along with a selection of corresponding major elements (calcium, silicon, aluminum, and phosphorus) and trace elements (copper, nickel, vanadium, and molybdenum) from XRF data. For major elements, calcium is a proxy for calcite, aluminum is a proxy for clay minerals, silicon is a general proxy for quartz plus feldspar, and phosphorus is a proxy for phosphate and low oxygenation. Among trace elements, copper and nickel are proxies for productivity, and vanadium and molybdenum are proxies for anoxia.

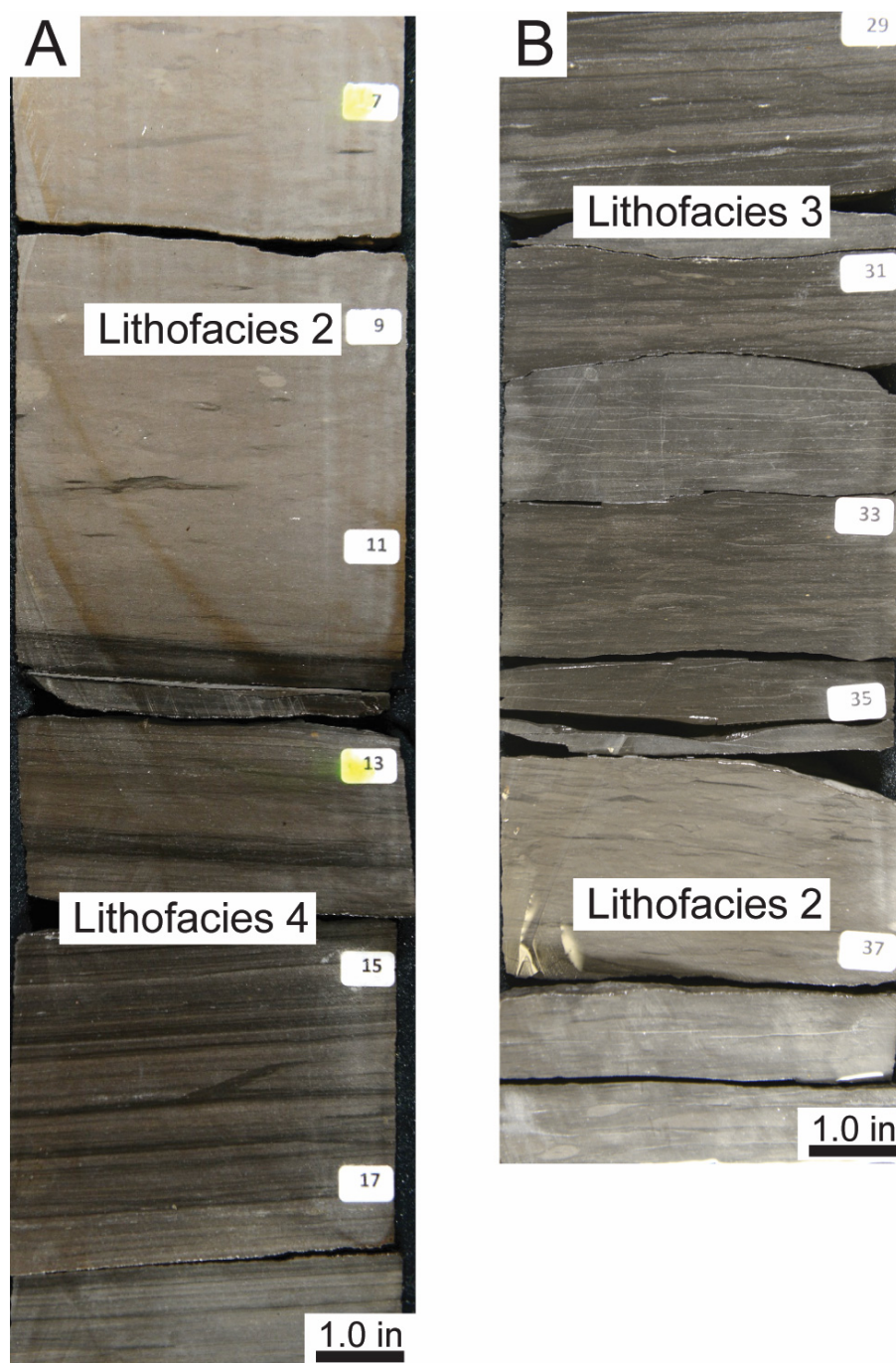


Figure 18. Small-scale depositional cycles. (A) Core slab showing lithofacies 4 well-laminated subcycle below lithofacies 2 burrowed subcycle. Sharp contact between two subcycles. Marathon Oil No. 1 Robert Todd (12,983.0 ft [3957.2 m]). (B) Core slab showing lithofacies 3 laminated subcycle above lithofacies 2 burrowed subcycle. Sharp contact between two subcycles. Marathon Oil No. 1 Robert Todd (12,985.0 ft [3957.8 m]). (C, [FACING PAGE](#)) XRF plot of major and trace elements versus depth in Robert Todd core. Elemental analyses clearly define cycles. Si + Al defines organic-matter-rich, laminated siliciclastic layers (lithofacies 4) and Ca defines organic-matter-poor, burrowed carbonate-rich layers (lithofacies 2).

See [Tribovillard et al. \(2006\)](#) for an in-depth discussion of using chemical proxies for paleoredox and paleoproductivity analysis. Calcite-rich units in the plot ([Fig. 18](#)) are lithofacies 2 with abundant horizontal burrows representing oxic to dysoxic deposition, and aluminum- and silicon-rich units are lithofacies 3 and 4 with laminae indicating anoxic deposition.

Lithofacies 2 is predominantly calcite (high calcium) with reduced quartz, feldspar, and clay minerals (silicon and alumi-

num) ([Fig. 18C](#)). Phosphorus, vanadium, and molybdenum spikes ([Fig. 18C](#)) are associated with lithofacies 4 and support deposition under anoxic bottom conditions. Copper and nickel showing elevated values ([Fig. 18C](#)) are also associated with lithofacies 4, suggesting periods of high productivity commonly associated with anoxic conditions in sea water. These small-scale cycles, therefore, denote the alternation between oxic to dysoxic or anoxic cycles.

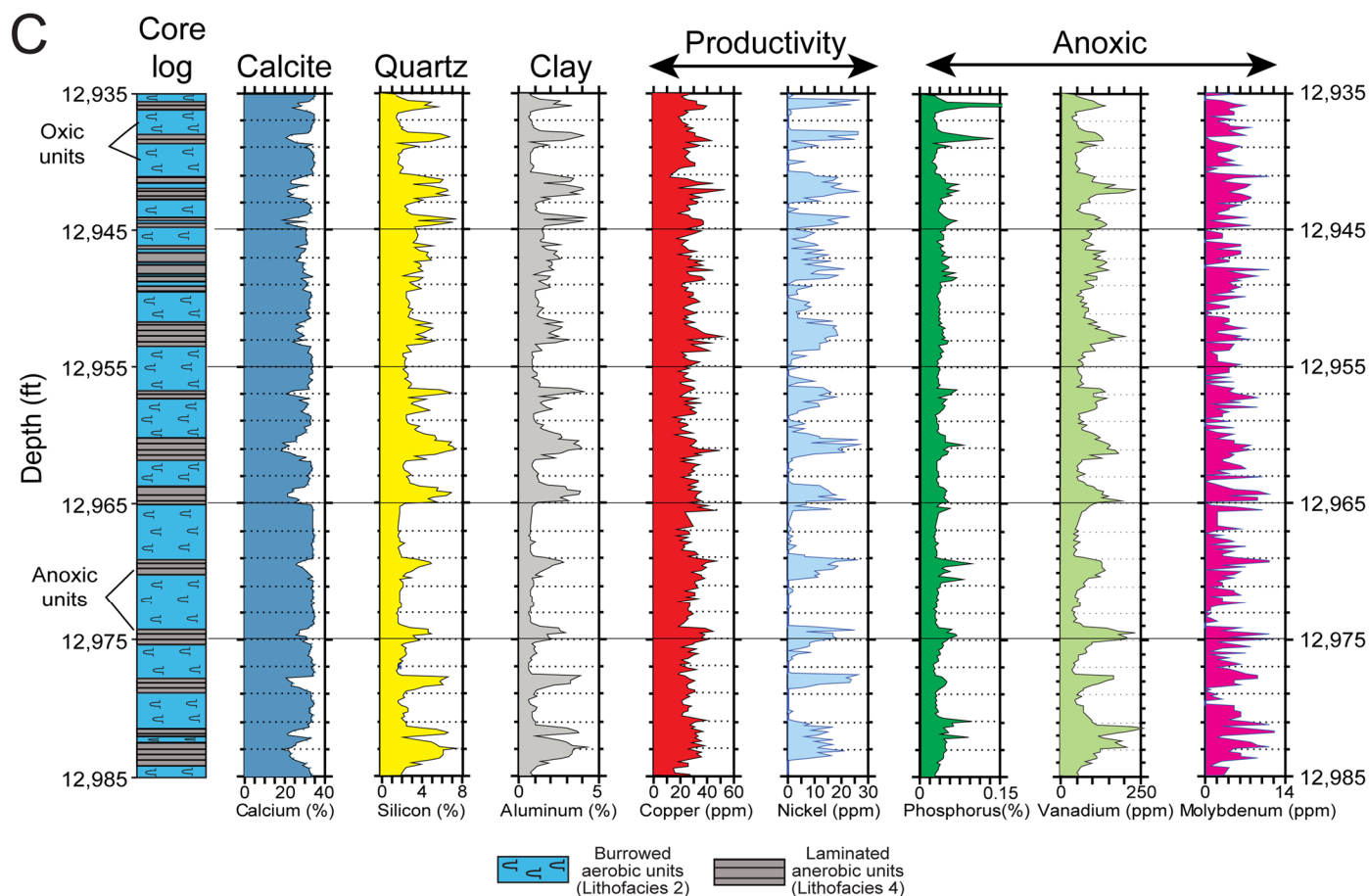


Figure 18, continued. (C) XRF plot of major and trace elements versus depth in Robert Todd core. Elemental analyses clearly define cycles. Si + Al defines organic-matter-rich, laminated siliciclastic layers (lithofacies 4) and Ca defines organic-matter-poor, burrowed carbonate-rich layers (lithofacies 2).

The base of the anoxic units is generally sharp (Fig. 18B), indicating a rapid change in bottom-water and chemical-sediment conditions. The sharp contact (i.e., not burrowed) can be attributed to anoxic conditions in lithofacies 3 and 4 inhibiting most bioturbation, which could have affected the lower contact. The upper contact of the anoxic units ranges from sharp to well burrowed (Fig. 18A). The burrowed contact resulted from bioturbation by organisms living in the oxic to dysoxic sediments above. These burrowing organisms lived in the more oxygenated sediments and ventured down into the organic-rich sediments below; however, because they could only tolerate the upper part of the anoxic sediments, only the top of the anoxic sediment unit was bioturbated.

The multiple rhythmic stacking of these small-scale cycles suggests a relatively short-term, repeatable change in environmental (i.e., chemical) conditions, and these short-term cycles may be Milankovitch cycles (i.e., orbital, forced cycles) that are commonly observed in many of the Upper Cretaceous chalks worldwide, including the Austin-equivalent Niobrara Chalk in the Western Interior Seaway (Locklair and Sageman, 2008). Eldrett et al. proposed these astronomical forcing Milankovitch cycles for the Eagle Ford Group in South Texas. The orbital, forced cycles documented by Locklair and Sageman (2008) are thought to be related to eccentricity (100, 400, and 1000 kyr), obliquity (41 kyr), and precession (21 kyr). The rhythmic cycles in the Louisiana Austin Chalk Group most likely had the same durations as did the cycles seen in the Niobrara Chalk. Further

work is necessary, however, to document an orbital control for the rhythmic stacking patterns observed in the Austin Chalk.

PORE NETWORKS AND RESERVOIR QUALITY

Pore Types and Pore Networks

The character and connectedness of pore spaces and resulting reservoir quality are important geologic characteristics relative to developing exploration and exploitation concepts, especially for unconventional reservoirs. The Austin Chalk reservoirs are tight carbonates with matrix permeabilities generally less than 0.001 md based on modified gas-expansion analyses. Because of this low matrix reservoir quality, high rates of production are dependent on fractures (Fig. 19A). Also, to characterize the matrix reservoir quality, special attention needs to be focused on pore types and pore networks (Fig. 19).

This investigation used the mudrock pore-type classification developed by Loucks et al. (2012). The Austin Chalk mineralogy and texture indicates that it is a siliciclastic-rich carbonate mudrock; thus, this pore classification well defines the type of nano- to micropores seen in the chalk (Figs. 19B–19J). Terminology for organic-matter pores is after Reed et al. (2020).

The dominant pore type in the Austin Chalk is interparticle nanopores ranging between tens to approximately 1000 nanometers, with the interparticle nanopores occurring predominantly between coccolith elements (Figs. 19B–19E). Many interparticle

nanopores are segmented by clay platelets (Figs. 19C–19F) that decrease permeability by reducing pore-throat sizes. These interparticle nanopores are probably well connected by nanopore throats.

There are several types of intraparticle pores, although they are much less abundant than interparticle nanopores. Intraparticle nanopores occur within clay platelets (Figs. 19E and 19F) and as inherited nanopores in inoceramid fragments (Fig. 19G). Pyrite framboids can also have intraparticle nanopores between their crystal elements.

Organic-matter (OM) nanopores are present in solid bitumen in higher, thermally mature ($R_o > 0.7\%$) strata (e.g., No. 17–1 Quinn; Figs. 19H–19J). They range in size from 10 to 1000 nanometers. Spongy and bubble nanopores form during the maturation of liquid bitumen to solid bitumen (Loucks et al., 2009; Loucks et al., 2013; Ko et al., 2017; Reed et al., 2020). Modified mineral pores form by liquid bitumen entering a pore space occupied by water, but the liquid bitumen does not displace all the water leaving a water-filled pore rimmed by bitumen (Ko et al., 2017; Reed et al., 2020).

In less thermally mature ($R_o < 0.7\%$) cores (No. 1 Donner, No. 1 Cabra, and No. 1 Robert Todd), the pore network appears to be predominantly interparticle nanopores, with some intraparticle nanopores (e.g., Fig. 19C). In higher, thermally mature ($R_o > 0.7\%$) cores (No. 1 Singletary, No. 1C Musser Davis, and No. 17–1 Quinn), the pore network is predominantly interparticle nanopores, with some OM nanopores and fewer intraparticle nanopores (e.g., Fig. 19H–19J).

Reservoir Quality

Even with several measurement techniques available, it is not a simple process to summarize reservoir quality – porosity and permeability. Studies now in progress by several of the present authors on Austin Chalk reservoir quality, reveal that conventional core-plug analysis cannot adequately measure porosity, and especially permeability of these relatively tight Austin Chalk strata. GRI-technique crushed rock analysis is better but also is not accurate. Special core analysis protocols, such as those developed by Peng and Loucks (2016) and Peng et al. (2019), are necessary to measure reservoir quality in Austin Chalk strata accurately. Limited analyses of each method are presented.

One-hundred-thirty conventional core-plug analyses are available from the No. 1 Sonat B6, No. 1 Singletary, and No. 1C Musser Davis cores (Figs. 20A and 20B). Lithofacies 1 has the highest porosities (many between 7–9%) (Fig. 20A), with lithofacies 2–4 showing a similar porosity range between 2 and 6%. Permeability displays no relationship with porosity and is generally less than 0.2 md (Fig. 20A). The geometric mean permeability of all lithofacies is low (0.015 – 0.029 md) (Fig. 20A). Also, note that no individual permeability values present lower than 0.001 md (Fig. 20A). This is related to the inability of conventional core-plug-analysis methods to measure lower values. Ongoing studies by several of the present authors show that conventional core-plug analyses are optimistic, especially permeability values.

Figure 20C is a table showing mean values of GRI crushed-rock porosity analyses for the No. 1 Cabra and No. 1 Singletary cores. Permeability was not measured. Mean GRI crushed-rock porosity in the two wells are similar to conventional core-plug porosity in the No. 1 Sonat B6, No. 1 Singletary, and No. 1C Musser Davis cores (5.9% versus 5.0%, respectively). The highest mean porosity is in lithofacies 4 (Fig. 20C), whereas, with the conventional core-plug porosity analysis, lithofacies 1 has the highest mean porosity.

The modified gas-expansion (MGE) method for porosity and permeability in the No. 1 Cabra core for 13 analyses is shown in Figure 20D and 20E. The MGE method provides the ability to measure permeability in the low nanodarcy range (as low as 5.6

nd; Figs. 20D and 20E). Mean porosity is similar to conventional core-plug, and GRI crushed rock porosities; however, geometric mean permeability by the MGE method is much lower (0.00018 md) by two orders of magnitude than the conventional core-plug method (0.012 md). This disparity in permeabilities related to analytical methods is documented in other cores by several of the present authors. Interestingly, the MGE method shows a strong correlation between porosity and log permeability ($R = 0.91$) (Fig. 20D).

All three methods indicate that matrix permeability in the Austin Chalk strata is very low. Based on these analyses, porosities <10% and permeabilities <0.05 md (optimistic) should be expected in the producing trend.

CONCLUSIONS

This Austin Chalk investigation in the producing trend in Louisiana has defined “working” stratigraphic picks within the section based on wireline logs and cores (Fig. 7). The TAC and BAC horizons reflect changes in lithology and cycle development with adjacent units.

The Austin Chalk is a siliciclastic-rich chalk, and mineralogy is dominated by calcite, a product of biological production of mainly coccolithophores and foraminifers. Siliciclastic components are abundant (5–40% on average) in which the clay-mineral/quartz plus feldspar ratio is ~9:1 (Fig. 6).

Biotic components are predominantly coccolithophore fragments, planktic foraminifers, and calcispheres that lived in the shallower-water column in an open-marine environment. Following death, planktic biotas settled out of suspension to the seafloor, mainly as ‘marine snow’ and peloids. Inoceramids were the only common fauna that lived on the seafloor during lower oxygen conditions. Much rarer benthic foraminifers, echinoderms, oysters, and ostracods have been noted in the more oxygenated strata.

Five general lithofacies were defined for the Austin Chalk. Lithofacies 1 is a highly bioturbated, organic-matter-poor marly chalk and rarer pure chalk, the general depositional setting being an open-marine, outer-shelf area below storm wave base. This area was far enough seaward of any land mass that sand-size siliciclastic sediment did not reach the area. Bottom waters and sediments were oxic, although at times slightly stressed, as indicated by the sparsity of benthic foraminifera. Lithofacies 2 is a highly bioturbated, organic-matter-poor to -rich marly chalk to chalky marl. As with lithofacies 1, the general depositional setting was in an open-marine, outer-shelf setting below storm wave base. The increased TOC present suggests that bottom waters and sediments were oxic to dysoxic; higher siliciclastic percentages suggest limitations in the productivity of the shallow water column as well. Lithofacies 3 is a slightly burrowed, organic-matter-rich, laminated marly chalk to lesser chalky marl. Bottom-water and sediment conditions illustrate a distinct change to dysoxic to anoxic environments, given the preponderance of laminated sediments, high TOC, and abundant pyrite. The depositional setting continued to be in an open-marine, outer-shelf environment below storm wave base. Lithofacies 4 is an organic-matter-rich, well-laminated marly chalk. The depositional setting is similar to lithofacies 3, but the total lack of bioturbation suggests a strongly anoxic bottom-water setting.

Austin Chalk strata contain numerous small-scale cycles composed of organic-matter-poor, burrowed units alternating with organic-matter-rich, laminated units. These small-scale cycles are thought to be Milankovitch cycles, which are also common in the time-equivalent Niobrara Chalk in the Western Interior Seaway. In the southwest and east part of the study area, the Austin Chalk shows a dysoxic to anoxic sedimentary wedge. We think that the wedge is related to a deepening of the water column and an increasing restriction as distance from the shal-

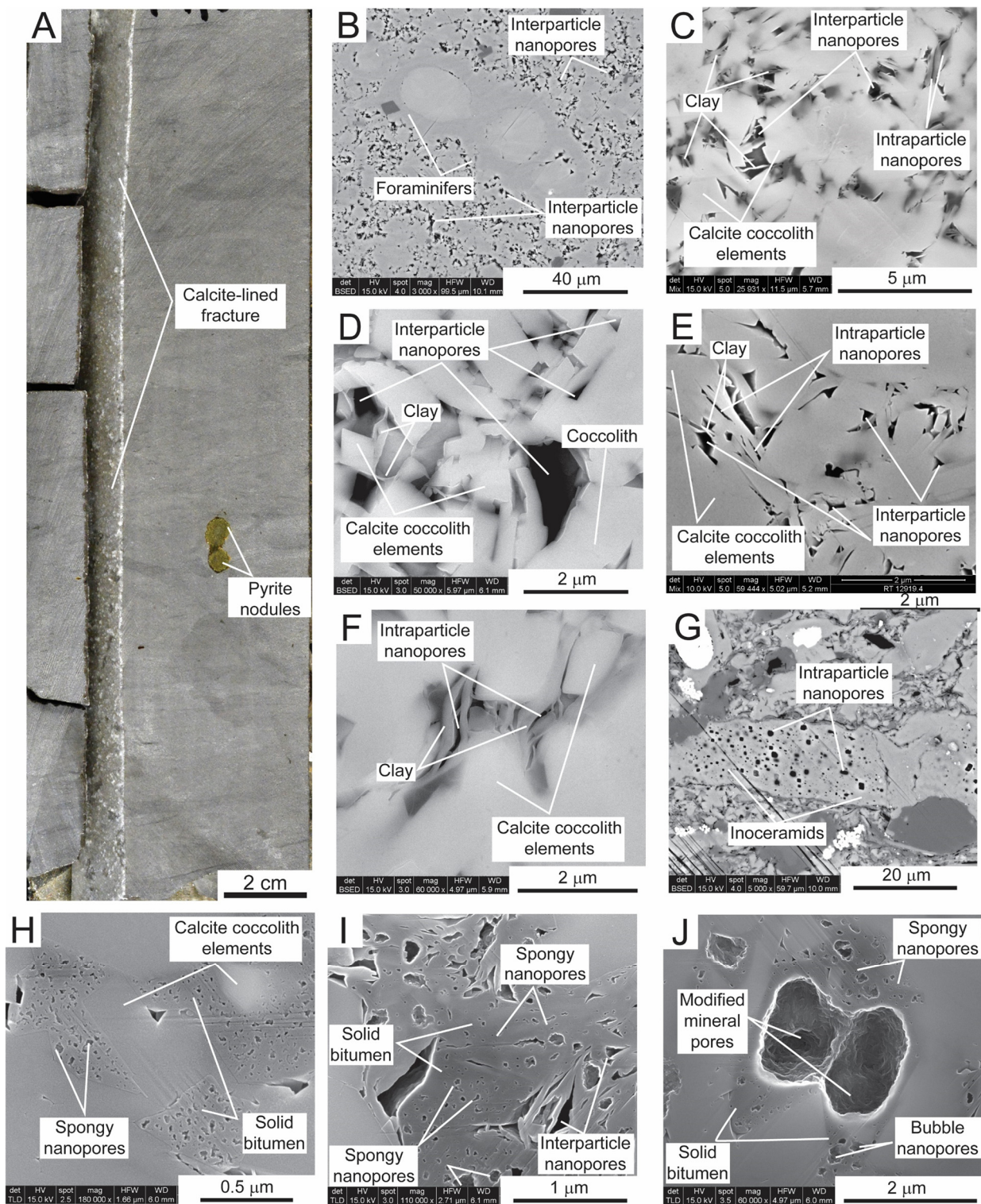


Figure 19. Pore types. (A) Natural fracture lined with calcite cement. Union Pacific Resources B6 No. 1 Sonat Minerals (14,378.0 ft [4373.3 m]). (B) Abundant interparticle nanopores between coccolith elements. Nanopores indicated by back specks in matrix. Union Pacific Resources B6 No. 1 Sonat Minerals (14,331.8 ft [4373.3 m]). (C) Interparticle nanopores between coccolith elements. Some clay-mineral platelets divide interparticle nanopores into smaller pores. Marathon Oil No. 1 Robert Todd (12,974.0 ft [3954.5 m]). (D) Interparticle nanopores between coccolith elements. Some clay-mineral platelets divide interparticle nanopores into smaller pores. Union Pacific Resources No. 17-1 Quinn (15,216.4 ft [4638.0 m]). (E) Interparticle nanopores between coccolith elements, and intraparticle nanopores within clay-mineral platelets. Marathon Oil No. 1 Robert Todd (12,919.4 ft [3937.8 m]). (F) Intraparticle nanopores between clay-mineral platelets. Union Pacific Resources No. 17-1 Quinn (15,216.7 ft [4638.4 m]). (G) Intraparticle nanopores within inoceramid fragment. Union Pacific Resources B6 No. 1 Sonat Minerals (14,400.1 ft [4389.2 m]). (H) Organic-matter spongy nanopores in solid bitumen that filled primary interparticle pore space between coccolith elements. Union Pacific Resources No. 17-1 Quinn (15,242.8 ft [4646.0 m]). (I) Organic-matter spongy nanopores within solid bitumen. Union Pacific Resources No. 17-1 Quinn (15,216.4 ft [4638.0 m]). (J) Image contains a spectrum of organic-matter nanopores within solid bitumen. Union Pacific Resources B6 No. 1 Sonat Minerals (14,330.7 ft [4368.0 m]).

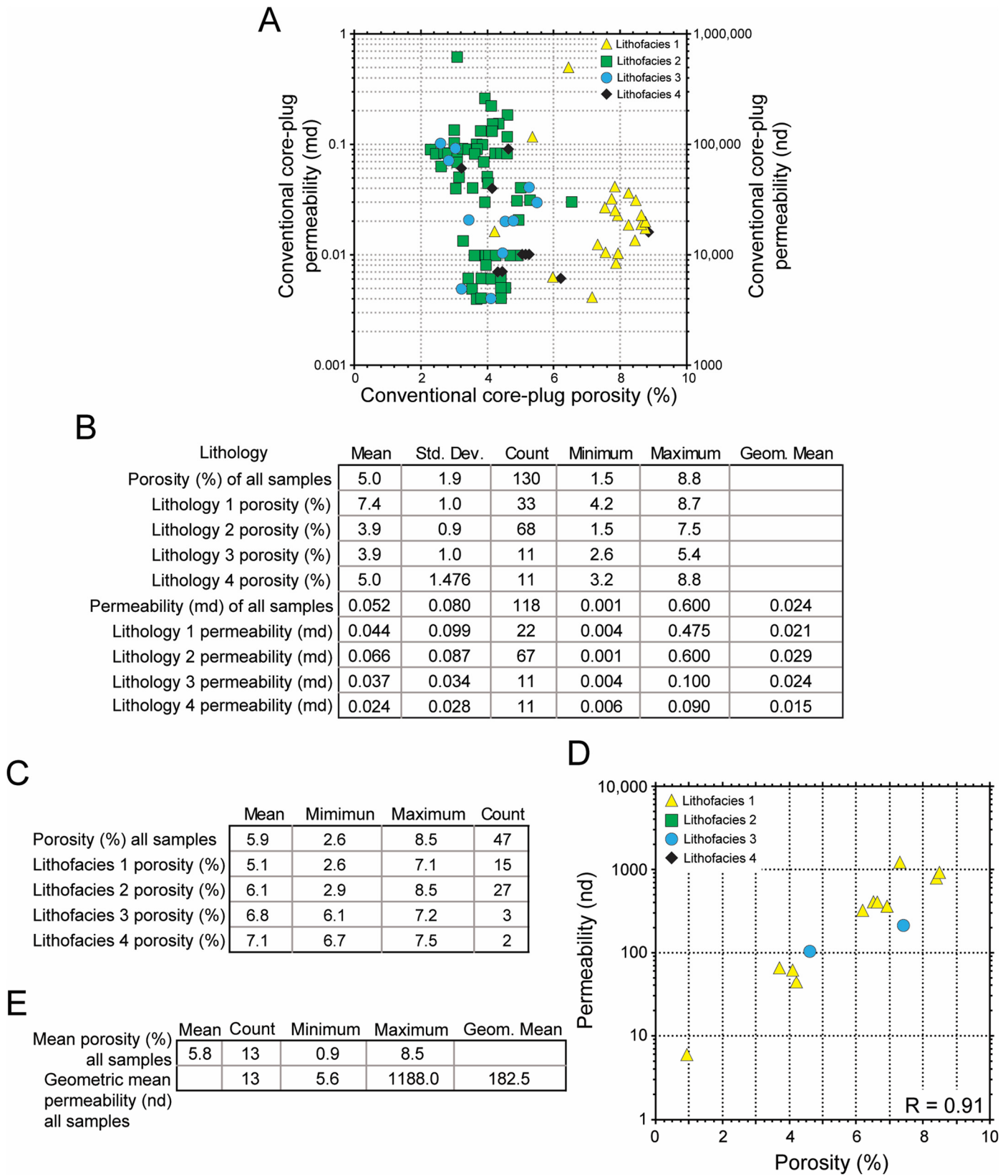


Figure 20. Reservoir quality data. (A) Porosity versus permeability plot of conventional core-plug data separated by lithofacies for the No.1 Sonat B6, No. 1 Singletary, and No. 1C Musser Davis cores. (B) Table of conventional core-plug porosity and permeability separated by lithofacies for the No.1 Sonat B6, No. 1 Singletary, and No. 1C Musser Davis cores. (C) Table of GRI crushed rock porosity data separated by lithofacies for the No. 1 Cabra and No. 1 Singletary cores. (D) Porosity versus permeability plot of modified gas expansion analyses separated by lithofacies for the No. 1 Cabra core. (E) Table of porosity and permeability separated by lithofacies for modified gas expansion analyses for the No. 1 Cabra core.

lower water Sabine Uplift area to the outer shelf increased (Fig. 3).

TOC content can be high (in the range of 2 to 7 wt%) and the source rock richness of many samples in lithofacies 2 to 4 plots in the fair to excellent range relative to S1 + S2. Lithofacies 1 is relatively low in TOC (mean 0.32 wt%), but some values are relatively high for carbonates deposited in oxic environments. Lithofacies 1 contains type III kerogen, whereas lithofacies 2 has both Type II and Type III kerogen, while lithofacies 3 and 4 are predominately Type II kerogen. These organic matter characteristics strongly suggest the Austin Chalk strata are in part self-sourcing.

The pore network within the Austin Chalk is dominated by interparticle nanopores that occur between coccolith elements. Additional pores are in the form of intraparticle nanopores within clay platelets and in inoceramid prisms. Organic-matter nanopores formed in solid bitumen in areas where the Austin Chalk reached thermal maturity values exceeding 0.7% R_o .

This investigation of the Austin Chalk provides concepts of current research interest that help to understand the depositional processes of siliciclastic-rich chalks. It also provides data on geological characteristics that should be of value in exploration and exploitation of siliciclastic-rich chalks.

ACKNOWLEDGMENTS

We want to recognize the Carbonate Reservoir Characterization Research Laboratory (RCRL) at the Bureau of Economic Geology and associated sponsors for support of this investigation. We appreciate the reviews of the manuscript by Lowell Waite, Alexis Godet, Tom Ewing, and Kim Patty. Lana Dieterich of the Bureau of Economic Geology edited an earlier version of this manuscript, and we recognize and appreciate her effort. We appreciate the data provided and discussions with Mike Cervantes (Continental Resources), Kim Patty (Chesapeake Energy), David Hull (Devon Resources), and Paul Mescher (independent consultant). Evan Sivil and Harry Rowe helped collect the XRF data. Mary Kamat of Marathon provided help with some of the wireline-log picks. Publication authorized by the Director, Bureau of Economic Geology, Jackson School of Geosciences, University of Texas at Austin.

REFERENCES CITED

- Allredge, A. L., and M. W. Silver, 1988, Characteristics, dynamics and significance of marine snow: *Progress in Oceanography*, v. 20, p. 41–42, <[https://doi.org/10.1016/0079-6611\(88\)90053-5](https://doi.org/10.1016/0079-6611(88)90053-5)>.
- Anderson, E. G., 1979, Basic Mesozoic study in Louisiana, the northern coastal region and the Gulf Basin Province: Louisiana Geological Survey Department of Natural Resources Folio Series 3, Baton Rouge, 58 p.
- Barker, D. S., and K. P. Young, 1979, A marine Cretaceous nepheline basanite volcano at Austin, Texas: *Texas Journal of Science*, v. 31, p. 5–24.
- Balch, W. M., 2004, Re-evaluation of the physiological ecology of coccolithophores, in H. R. Thyestean and J. R. Young, eds., *Coccolithophores—From molecular processes to global impact*: Springer-Verlag, New York, p. 165–190.
- Barnes, S., 2019, Enthusiasm for Louisiana's shale play has waned, but there's still hope for drilling: Greater Baton Rouge Business Report, <<https://www.businessreport.com/newsletters/enthusiasm-for-louisianas-shale-play-has-waned-but-theres-still-hope-for-drilling>>.
- Bé, A. W. H., 1960, Ecology of recent planktonic foraminifera, part 2, bathymetric and seasonal distributions in the Sargasso Sea off Bermuda: *Micropaleontology*, v. 6, p. 373–392.
- Bergen, J. A., and P. J. Sikora, 1999, Microfossil diachronism in southern Norwegian North Sea chalks, in R. W. Jones and M. D. Simmons, eds., *Biostratigraphy in production and development geology*: Geological Society, London, Special Publications, v. 152, p. 85–111, <<https://doi.org/10.1144/GSL.SP.1999.152.01.06>>.
- Blakey, R., 2011, Western North America series: Colorado Plateau Geosystems, Inc., <<http://www.cpgeosystems.com/paleomaps.html>>.
- Boucot, A. J., 1990, *Evolutionary paleobiology of behavior and coevolution*: Elsevier Science Publishers, Amsterdam–Oxford–New York–Tokyo, 724 p.
- Broerse, A. T. C., P. Ziveri, J. E. van Hinte, and S. Honjo, 2000, Coccolithophore export production, seasonal species composition and coccolith-CaCO₃ fluxes in the NE Atlantic (34°N 21°W and 48°N 21°W): *Deep-Sea Research II*, v. 47, p. 1877–1905.
- Clark, W. J., 1995, Depositional environments, diagenesis, and porosity of Upper Cretaceous volcanic-rich Tokio sandstone reservoirs, Haynesville Field, Claiborne Parish, Louisiana: *Gulf Coast Association of Geological Societies Transactions*, v. 45, p. 127–134.
- Cooper, J. R., A. G. Godet, and M. C. Pope, 2020, Tectonic and eustatic impact on depositional features in the upper Cretaceous Austin Chalk Group of south-central Texas, USA: *Sedimentary Geology*, v. 401, 17 p., <<https://doi.org/10.1016/j.sedgeo.2020.105632>>.
- Dawson, W. C., B. Katz, and V. D. Robison, 1995, Austin Chalk (!) petroleum system Upper Cretaceous, southeastern Texas: A case study: *Gulf Coast Association of Geological Societies Transactions*, v. 45, p. 157–163.
- Dawson, W. C., and E. F. Reaser, 1990, Trace fossils and paleoenvironments of Lower and Middle Austin Chalk (Upper Cretaceous), north-central Texas: *Gulf Coast Association of Geological Societies Transactions*, v. 40, p. 161–173.
- Dennen, K. O., and P. C. Hackley, 2012, Definition of Greater Gulf Basin Lower Cretaceous and Upper Cretaceous Lower Cenomanian Shale Gas Assessment Unit, United States Gulf of Mexico Basin onshore and state waters: *American Association of Petroleum Geologists Search and Discovery Article 10429*, Tulsa, Oklahoma, 37 p.
- Dravis, J. J., 1979, *Sedimentology and diagenesis of Upper Cretaceous Austin Chalk Formation, South Texas and northern Mexico*: Ph.D. Dissertation, Rice University, Houston, Texas, 512 p.
- Eldrett, J. S., C. Ma, S. C. Bergman, A. Ozkan, D. Minisini, B. Lutz, S.-J. Jackett, C. Macaulay, and A. E. Kelly, 2015, Origin of limestone-marlstone cycles: Astronomic forcing of organic-rich sedimentary rocks from the Cenomanian to early Coniacian of the Cretaceous Western Interior Seaway, USA: *Earth and Planetary Science Letters*, v. 423, p. 98–113, <<https://doi.org/10.1016/j.epsl.2015.04.026>>.
- Ewing, M., and E. M. Thorndike, 1965, Suspended matter in deep ocean water: *Science*, v. 147, 1291–1294, <<https://doi.org/10.1126/science.147.3663.129>>.
- Ewing, T. E., and S. C. Caran, 1982, Late Cretaceous volcanism in South and Central Texas—Stratigraphic, structural, and seismic models: *Gulf Coast Association of Geological Societies Transactions*, v. 32, p. 137–145.
- Fabricius, I. L., 2007, Chalk: Composition, diagenesis and physical properties: *Bulletin of the Geological Society of Denmark*, v. 55, p. 97–128.
- Flügel, E., 2004, *Microfacies of carbonate rock: Analysis, interpretation and application*: Springer-Verlag, Berlin, Germany, 976 p.
- Goddard, D. A., 2001, *Quick look handbook onshore Louisiana petroleum producing formations*: Louisiana State University Center of Energy Studies, Baton Rouge, <https://www.lsu.edu/ces/publications/2001/quick_look.pdf>.
- Guerreiro, C. V., 2013, *Paleoecology of coccolithophores in the submarine canyons of the central Portuguese continental margin: environmental, sedimentary and oceanographic implications*: Ph.D. Dissertation, University of Lisbon, Portugal, 251 p.
- Hattin, D. E., 1975, Petrology and origin of fecal pellets in Upper Cretaceous strata of Kansas and Saskatchewan: *Journal of Sedimentary Research*, v. 45, p. 686–696.
- Hovorka, S. D., and H. S. Nance, 1994, Dynamic depositional and early diagenetic processes in a deep-water shelf setting, Upper

- Cretaceous Austin Chalk, North Texas: Gulf Coast Association of Geological Societies Transactions, v. 44, p. 269–276.
- Hüneke, H., and R. Henrich, 2011, Pelagic sedimentation modern and ancient oceans, in H. Hüneke and T. Mulder, eds., Deep-sea sediments: Development in Sedimentology, v. 63, p. 353–396, <[https://doi.org/10.1016/S0070-4571\(11\)63004-5](https://doi.org/10.1016/S0070-4571(11)63004-5)>.
- Ko, L. T., R. G. Loucks, S. C. Ruppel, T. Zheng, and S. Peng, 2017, Origin and characterization of Eagle Ford pore networks in the South Texas Upper Cretaceous shelf: American Association of Petroleum Geologists Bulletin, v. 101, p. 387–418.
- Locklair, R. E., and B. B. Sageman, 2008, Cyclostratigraphy of the Upper Cretaceous Niobrara Formation, Western Interior, U.S.A.: A Coniacian–Santonian orbital timescale: Earth and Planetary Science Letters, v. 269, p. 540–553, <<https://doi.org/10.1016/j.epsl.2008.03.021>>.
- Loucks, R. G., 2018, Eagle Ford-A (Boquillas-A) depositional setting and processes in southwest Texas: An example of deeper-water, below-storm-wave base carbonate sedimentation on a drowned shelf: Gulf Coast Association of Geological Societies Journal, v. 7, p. 59–78.
- Loucks, R. G., G. Frébourg, and H. D. Rowe, 2017, Upper Cretaceous (Campanian) Ozan and Annona Chalks in Caddo—Pine Island Field, northwest Louisiana: Depositional setting, lithofacies, and nanopore/micropore network: Gulf Association of Geological Societies Journal, v. 6, p. 73–91.
- Loucks, R. G., B. G. Gates, and C. K. Zahm, 2019, Depositional systems, lithofacies, nanopore to micropore matrix network, and reservoir quality of the Upper Cretaceous (Cenomanian) Buda Limestone in Dimmit County, southwestern Texas: Gulf Association of Geological Societies Journal, v. 8, p. 271–300.
- Loucks, R. G., J. R. Lambert, K. Patty, T. E. Larson, R. M. Reed, and C. K. Zahm, 2020a, Regional overview and significance of the mineralogy of the Upper Cretaceous Austin Chalk Group, onshore Gulf of Mexico: Gulf Coast Association of Geological Societies Journal, v. 9, p. 1–16.
- Loucks, R. G., T. E. Larson, Y. Z. Zheng, C. K. Zahm, L. T. Ko, Sivil, J. E., P. Sheng, S. C. Ruppel, and W. A. Ambrose, 2020b, Geologic characterization of the type cored section for the Upper Cretaceous Austin Chalk Group in South Texas: A combination fractured and unconventional reservoir: American Association of Petroleum Geologists Bulletin, v. 104, p. 2209–2245, <<https://doi.org/10.1306/04222019197>>.
- Loucks, R. G., R. M. Reed, L. T. Ko, C. K. Zahm, and T. E. Larson, 2021, Micropetrographic characterization of a siliciclastic-rich chalk; Upper Cretaceous Austin Chalk Group along the onshore northern Gulf of Mexico, USA: Sedimentary Geology, v. 412, 19 p., <<https://doi.org/10.1016/j.sedgeo.2020.105821>>.
- Loucks, R. G., R. M. Reed, S. C. Ruppel, and U. Hammes, 2012, Spectrum of pore types and networks in mudrocks and a descriptive classification for matrix-related mudrock pores: American Association of Petroleum Geologists Bulletin, v. 96, p. 1071–1098, <<https://doi.org/10.1306/08171111061>>.
- Loucks, R. G., R. M. Reed, S. C., Ruppel, and D. M. Jarvie, 2009, Morphology, genesis, and distribution of nanometer-scale pores in siliceous mudstones of the Mississippian Barnett Shale: Journal of Sedimentary Research, v. 79, p. 848–861, <<https://doi.org/10.2110/jsr.2009.092>>.
- Louisiana Geological Survey, 2019, Shale and chalk plays in Louisiana, a brief historical review, current activity summary, future potential, in Louisiana Oil and Gas Symposium—April 2019, shale and chalk plays in Louisiana, <https://www.lsu.edu/lgs/conferences/laoilgas2019/laoilgas2019_stamatades.pdf>.
- McGinnis, R. N., D. A. Ferrill, A. P. Morris, K. J. Smart, and D. Lehrmann, 2017, Mechanical stratigraphic controls on natural fracture spacing and penetration: Journal of Structural Geology, v. 95, p. 160–170, <<https://doi.org/10.1016/j.jsg.2017.01.001>>.
- Moore, R. C., 1967, Unique stalked crinoids from Upper Cretaceous of Mississippi: University of Kansas Paleontological Contributions, Paper 17, 35 p., <<hdl.handle.net/1808/3676>>.
- Moore, D. M., and R. C. Reynolds, 1997, X-ray diffraction and the identification and analysis of clay minerals, 2d ed.: Oxford University Press, U.K., 332 p.
- Mulder, T., and J. Alexander, 2001, The physical character of subaqueous sedimentary density flows and their deposits: Sedimentology, v. 48, p. 269–299, <<https://doi.org/10.1046/j.1365-3091.2001.00360.x>>.
- Passwaters, M., 2018, Quiet for decades, Austin Chalk oil and gas play attracting new interest: S&P Global Market Intelligence, <<https://www.spglobal.com/marketintelligence/en/news-insights/trending/a1nz8ucyjoszmjxzykxw2>>.
- Pearson, K., 2012, Geologic models and evaluation of undiscovered conventional and continuous oil and gas resources—Upper Cretaceous Austin Chalk, U.S. Gulf Coast: U.S. Geological Survey Scientific Investigations Report 2012–5159, 26 p.
- Peng, S., and R. G. Loucks, 2016, Permeability measurements in mudrocks using gas-expansion methods on plug and crushed-rock samples: Marine and Petroleum Geology, v. 73, p. 299–310, <<https://doi.org/10.1016/j.marpetgeo.2016.02.025>>.
- Peng, S., B. Ren, and M. Meng, 2019, Quantifying the influence of fractures for more-accurate laboratory measurement of shale matrix permeability using a modified gas-expansion method: Society of Petroleum Engineers Paper SPE–195570–PA, Richardson, Texas, 12 p., <<https://doi.org/10.2118/195570-PA>>.
- Phelps, R. M., C. Kerans, R. G. Loucks, R. O. B. P. Da Gama, J. Jeremiah, and D. Hull, 2013, Oceanographic and eustatic control of carbonate platform evolution and sequence stratigraphy on the Cretaceous (Valanginian–Campanian) passive margin, northern Gulf of Mexico: Sedimentology, v. 62, p. 461–496, <<https://doi.org/10.1111/sed.12062>>.
- Ray, D. C., F. S. P. van Buchem, G. Baines, A. Davies, B. Gréselle, M. D. Simmons, and C. Robson, 2019, The magnitude and cause of short-term eustatic Cretaceous sea-level change: A synthesis: Earth-Science Reviews, v. 197, 20 p., <<https://doi.org/10.1016/j.earscirev.2019.102892>>.
- Reading, H. G., and J. D. Collinson, 1996, Clastic coasts, in H. G. Reading, ed., Sedimentary environments: Processes, facies and stratigraphy: Blackwell Science, Oxford, U.K., p. 154–131, <ISBN:978-0-632-03627-1>.
- Reed, R. M., R. G. Loucks, and L. T. Ko, 2020, Scanning electron microscope petrographic differentiation among different types of pores associated with organic matter in mudrock: Gulf Coast Association of Geological Societies, v. 9, p. 17–27.
- Roth, P. H., 1994, Distribution of coccoliths in oceanic sediments, in A. Winter and W. G. Siesser, eds., Coccolithophores: Cambridge University Press, U.K., p. 199–218.
- Rowe, H. D., N. Hughes, and K. Robinson, 2012, The quantification and application of handheld energy-dispersive X-ray fluorescence (ED-XRF) in mudrock chemostratigraphy and geochemistry: Chemical Geology, p. 324–325, 122–131, <<https://doi.org/10.1016/j.chemgeo.2011.12.023>>.
- Schieber, J., 2007, Microbial mats on muddy substrates—Examples of possible sedimentary features and underlying processes, in J. Schieber, P. Bose, P. G. Eriksson, S. Banerjee, S. Sarkar, W. Altermann, and O. Catuneanu, eds., Atlas of microbial mat features preserved within the siliciclastic rock record: Atlases in Geoscience 2, Elsevier, Amsterdam, The Netherlands, p. 117–134.
- Schieber, J., 2009, Discovery of agglutinated benthic foraminifera in Devonian black shales and their relevance for the redox state of ancient seas: Palaeogeography, Palaeoclimatology, Palaeoecology, v. 271, p. 292–300, <<https://doi.org/10.1016/j.palaeo.2008.10.027>>.
- Scholle, P. A., 1977, Chalk diagenesis and its relationship to petroleum exploration: Oil from chalks, a modern miracle?: American Association of Petroleum Geologists Bulletin, v. 61, p. 982–1009.
- South Carolina Oyster Recycling and Enhancement, 2020, Oyster geology & ecology, <<http://score.dnr.sc.gov/deep.php?subject=2&topic=15>>.
- Stanley, D. J., 1993, Model for turbidite-to-contourite continuum and multiple process transport in deep marine settings: Examples in the rock record: Sedimentary Geology, v. 82, p. 241–255, <[https://doi.org/10.1016/0037-0738\(93\)90124-N](https://doi.org/10.1016/0037-0738(93)90124-N)>.

- State of Louisiana Department of Natural Resources, 2018, Resurgence in Austin Chalk play, <<http://www.dnr.louisiana.gov/index.cfm/page/1442>>.
- Steinmetz, J. C., 1994, Sedimentation of coccolithophores, in A. Winter and W. Siesser, eds., *Coccolithophores*: Cambridge University Press, U.K., p. 179–230.
- Tribovillard, N., T. J. Algeo, T. Lyons, and A. Riboulleau, 2006, Trace metals as paleoredox and paleoproductivity proxies: an update: *Chemical Geology*, v. 232, p. 12–32, <<https://doi.org/j.chemgeo.2006.02.012>>.
- Vail, P. R., R. M. Mitchum, Jr., and S. Thompson III, 1977, Seismic stratigraphy and global changes of sea level, part 4: Global cycles of relative changes of sea level, in C. E. Payton, ed., *Seismic stratigraphy—Applications to hydrocarbon exploration*: American Association of Petroleum Geologists Memoir 26, Tulsa, Oklahoma, p. 83–97.
- van der Zwaan, G. J., F. J. Jorissen, and H. C. de Stigter, 1990, The depth dependency of planktonic/benthic foraminiferal ratios: constraints and applications: *Marine Geology*, v. 95, p. 1–16.
- Vink, A., 2004, Calcareous dinoflagellate cysts in South and equatorial Atlantic surface sediments: Diversity, distribution, ecology and potential for paleoenvironmental reconstruction: *Marine Micropaleontology*, v. 50, p. 43–88, <[https://doi.org/10.1016/S0377-8398\(03\)00067-7](https://doi.org/10.1016/S0377-8398(03)00067-7)>.
- Walker, J. D., J. W. Geissman, S. A. Bowring, and L. E. Babcock, compilers, 2018, *Geologic time scale*, v. 5.0: Geological Society of America, Boulder, Colorado.
- Williams, J. D., 1963, The petrology and petrography of sediments from the Sigsbee blanket, Yucatan Shelf, Mexico: American Petroleum Institute Project 63, Washington, D.C., and Texas A&M University Department of Oceanography and Meteorology Project 287A, Reference 63–12T, College Station, 60 p.
- Zborowski, M., 2019, Louisiana Austin Chalk: Hundreds of millions down the drain?: *Journal of Petroleum Technology*, <<https://pubs.spe.org/en/jpt/jpt-article-detail/?art=6039>>.
- Ziveri, P., A. T. C. Broerse, J. E. van Hinte, P. Westbroeck, and S. Honjo, 2000a, The fate of coccoliths at 48°N 21°W, north-eastern Atlantic: Deep-Sea Research Part II: Topical Studies in Oceanography, v. 47, p. 1853–1875, <[https://doi.org/10.1016/S0967-0645\(00\)00009-6](https://doi.org/10.1016/S0967-0645(00)00009-6)>.
- Ziveri, P., A. Ruttén, G. J. de Lange, J. Thomson, and C. Corselli, 2000b, Present-day coccolith fluxes recorded in central eastern Mediterranean sediment traps and surface sediments: *Palaeogeography, Palaeoclimatology, Palaeoecology*, v. 158, p. 175–195, <[https://doi.org/10.1016/S0031-0182\(00\)00049-3](https://doi.org/10.1016/S0031-0182(00)00049-3)>.